Final Report
RBCC Mixing Studies
NCC8-123

Executive Summary

Introduction:
The research project reported herein extended over a period from October 1997 through August 1999. The research resulted in three technical papers presented at the AIAA/SAE/ASME/ASEE 35th Joint Propulsion Conference in Los Angeles in July 1999. These three papers are attached to this Executive Summary to constitute the final report.

Objective:
The objective of this research was to determine the mixing characteristics between the primary rocket jets and the turbine exhaust stream in a simulated Rocket Based Combined Cycle propulsion concept operating in the air augmented rocket mode.

Summary:
The experiment was to model the Strutjet design of GenCorp Aerojet at a scale of no less than 1/6 the size of an engine for a vehicle that delivers a 25K lbm. payload to the International Space Station. The program was accomplished in three distinct phases, design of the experiment, flow visualization testing of the mixing process and pressure measurements to gain quantitative knowledge of the flow behavior in the ductwork.

The design of the experiment resulted in a cold flow test arrangement in which a Strutjet configuration with 2 simulated rocket nozzles and a single, vertically oriented, turbine exhaust nozzle between them. A square duct surrounding the Strutjet conveyed the ingested airflow from an inlet through the test section to an exit. This configuration was to be tested with air as the simulated rocket exhaust gas and carbon dioxide as the simulated turbine exhaust gas. The CO_2 was to be seeded with acetone that fluoresced when illuminated by a laser. The scaling parameter chosen was the convective Mach Number between the simulated rocket flow and the turbine exhaust flow.

The experimentation with this configuration resulted in a series of images that permitted direct viewing of the mixing process from the nozzle exits to a distance of about 10 equivalent nozzle diameters downstream. The ratio of the nozzle pressures at the point of intersection of the flows had a significant effect. Of the pressure ratios tested in this research, it seems that a turbine nozzle exhausting at about twice the pressure of the rocket jets, is the best combination for the air augmented operating mode. This delays the mixing of the turbine flow with the rocket flows the longest distance from the exit plane.

The ingested air in the duct was found to be choked. The pressure probes served to determine that this was the result of the area change at the strut rather than due to the mass addition by the jets. Additionally, the pressure probes served to yield information about the nature of shocks and the resulting flows throughout the mixing region.

Only one nozzle configuration was tested during this program. It is desirable to evaluate other nozzle configurations and turbine exhaust nozzle orientations to determine if there may be other means by which to control the mixing process to achieve the desired ends to maximize RBCC performance.

Papers & Articles Resulting from this Research:

1. Spetman, D. M., Hawk, C. W. and Moser, M. D., "*Development of a Strutjet Cold-Flow Mixing Experiment*", Journal of Propulsion and Power, Volume 15, Number 1,January-February 1999, pp. 155-158.
2. S. Muller, C. W. Hawk, P. G. Bakker, D. Parkinson and M. Turner, *"Mixing of Supersonic Jets in a RBCC Strutjet Propulsion System"*, Submitted to the AIAA *Journal of Propulsion and Power*, August 1999
3. Parkinson, D, Turner, M and Wagner, D, *"Mixing of Hypersonic Streams"*, **AIAA-Paper 99-2454**, AIAA/SAE/ASME/ASEE 35th Joint Propulsion Conference and Exhibit, Los Angeles, CA, June 1999
4. S. Muller, C. W. Hawk, P. G. Bakker, D. Parkinson and M. Turner, *"Mixing of Supersonic Jets in a RBCC Strutjet Propulsion System"*, **AIAA Paper 99-2973**, AIAA/SAE/ASME/ASEE 35th Joint Propulsion Conference and Exhibit, Los Angeles, CA, June 1999
5. Landrum, D. B., Thames, M., Parkinson, D., and Gautney, S., "Investigation of the Rocket Induced Flow Field in A Rectangular Duct," **AIAA-Paper 99-2100**, AIAA/SAE/ASME/ASEE 35th Joint Propulsion Conference and Exhibit, Los Angeles, CA, June 1999
6. Hawk, C. W., Landrum, D. B., Muller, S., Turner, M., and Parkinson, D., "Mixing of Supersonic Streams" 35th Combustion, Airbreathing Propulsion, Propulsion Systems Hazards Subcommittee Joint Meeting, Tucson, AZ, December 1998.
7. Hawk, C. W., Turner, M., Wagner, D. K., and Lambert, J., "Mixing of Supersonic Streams", 1998 JANNAF Propulsion Meeting, 15-17 July, 1998, Cleveland, OH
8. Hawk, C. W., Landrum, D. B., Spetman, D. M., and Parkinson, D., "Mixing of Supersonic Streams", 1997 JANNAF 34th Combustion Subcommittee, Propulsion Systems Hazards Subcommittee and Airbreathing Propulsion Subcommittee, Joint Meeting, October 1997

Development of a Strutjet Cold Flow Mixing Experiment

David M. Spetman*, Clark W. Hawk† and Marlow D. Moser‡
University of Alabama in Huntsville, Huntsville, AL 35899

Introduction

Rocket-Based Combined Cycle (RBCC) concepts attempt to improve the performance of launch vehicles at all points in the launch trajectory and make highly reusable launch vehicles a reality. The Strutjet RBCC concept consists of a variable geometry duct with vertical struts inside that function in ducted rocket, ramjet, scramjet, and pure rocket modes.[1] These struts have rocket and turbine exhaust nozzles imbedded within them. The rocket flows induce an ejector effect with the ambient air at subsonic flight velocities. In ramjet and scramjet modes, the fuel rich nozzle flows react with the ambient air producing an afterburner effect. As shown in Fig. 1, the four primary rocket flows exit at the end of the strut with three turbine exhaust nozzles in between them. The Strutjet is designed to mix the fuel rich flows (rocket and turbine exhaust gases) in the vertical direction before significant combustion occurs with the ambient air. After the hot, fuel rich flows are mixed (and after the shear layers between the nozzle flows and the ambient air reach the walls of the duct), air breathing combustion begins. The combustion products thermally choke and are expanded through the duct's nozzle which is provided by the engine and, to a large part, by the air frame.[2] The objective of this paper is to present the development of an experiment that will determine the mixing characteristics of the Strutjet rocket and turbine exhaust gases.

Approach

A scale model of the current Strutjet design will be cold flow tested in a duct. The simulants will be heated and the nozzles will be designed to match the convective Mach number predicted for the full scale Strutjet nozzle flows in order to obtain similar mixing. The turbine nozzle gas will be seeded in order to trace the mixing of the turbine simulant with the rocket simulant.

Constraints

The main constraints on the design of the experiment were the similarity parameter, matching the geometric scale of a subscale test motor, (one-sixth of an engine for a vehicle that delivers a 25K lbm. payload to the International Space Station) and the diagnostic technique. The parameter chosen to ensure mixing similarity between the model and full scale prototype was convective Mach number (Mc), developed by Papamoschou and Roshko in order to correlate supersonic shear layer growth rates.[3] A derived variable, the convective velocity (Uc), is used to approximate the velocity of the large turbulent structures found in supersonic shear layers. As shown in Equation 1, the convective velocity is calculated by weighting the velocities of two flows by the speeds of sound of the opposite flows and assumes: (1) similar specific heat ratios (Eqn. 1 is exact for $\gamma_1 = \gamma_2$), (2) equal total and static pressures at the shear layer, and (3) steady flow.

---

* Von Braun Propulsion Fellow, Propulsion Research Center, Department of Mechanical and Aerospace Engineering. Student Member AIAA.
† Director, Propulsion Research Center; Professor, Department of Mechanical and Aerospace Engineering. Fellow AIAA.
‡Assistant Research Professor, Propulsion Research Center, Department of Mechanical and Aerospace Engineering, Member AIAA

$$U_C \approx \frac{a_2 U_1 + a_1 U_2}{a_1 + a_2} \tag{1}$$

$$M_{C_1} = \frac{U_1 - U_C}{a_1} \approx M_{C_2} = \frac{U_C - U_2}{a_2} \tag{2}$$

This approach makes the convective Mach number a compressibility-effect parameter and creates a coordinate system based on the motion of the large, dominant structures seen in turbulent flow. The convective Mach number can be calculated using either of the two flows as a reference flow (see Eqn. 2); both methods are equal if both flows have the same specific heat ratio, are supersonic, and Mc < 0.4 (asymmetries become apparent above Mc = 0.4 because of compressibility effects).[4,5] In the full scale, hot flow Strutjet, the convective Mach number between the rocket and turbine flows (Mc_{rt}) is approximately 0.6. The convective Mach number between the rocket and ambient airflows is 2.6, and the convective Mach number between the turbine and ambient airflows is 2.0. Since the experiment is a cold flow test, the convective Mach numbers associated with the exhaust gases and ambient air are impossible to achieve; however, Mc_{rt} = 0.6 is possible, since it is a relative parameter between the hot rocket and turbine flows. Even then, the simulated rocket exhaust must be heated in order to achieve Mc_{rt} = 0.6. Because of this constraint, only the mixing between the rocket and turbine flows will be simulated with the experiment, and any contribution from ambient air mixing (and the ejector effect) will not be accurately simulated.

Optical Diagnostics

The overall goal of the diagnostics function is to provide both qualitative and quantitative information about the mixing behavior downstream of the strut rocket base. The quantitative results will provide a measure of the degree of mixing at various axial locations downstream of the strut rocket base while the qualitative information obtained will provide valuable information about the structure of the flow field. The design of the simulant supply systems and the geometry of the duct reflect the needs of the diagnostic technique that will be used on this project.

The potential methods investigated included Al_2O_3 seeding,[6] methanol/ethanol condensation,[7] and acetone fluorescence.[8] Al_2O_3 seeding was not chosen due to the increasing error from particle lag time the greater the distance from the nozzle exit. Methanol/ethanol was not chosen due to the possibility of droplet nucleation at the farthest sampling location. Acetone vapor fluorescence was chosen due to its strong signal properties and ease of seeding.

The acetone vapor is excited at a wavelength of 266 nm and the fluorescent signal is emitted over a wide spectral range (~350 nm to 550 nm). The fluorescent signal will be collected over a bandwidth of 485-495 nm, eliminating interference from scattered laser light. Acetone fluorescence is linear with respect to incident laser intensity and acetone mole fraction.[8] Collision quenching of acetone fluorescence is intra molecular[8]. The fluorescence is, therefore, independent of temperature and local gas composition. Thus, quantitative information is readily obtained from the collected images.

The acetone fluorescence has a lifetime of less than 4 nanoseconds. Acetone also phosphoresces at wavelengths similar to the fluorescence, albeit at a much greater lifetime of about 200 microseconds. The phosphorescence interference is rendered negligible by the gating of the intensified camera at 10 microseconds. This also eliminates background interference

The Nd:YAG laser output of 1064 nm is frequency quadrupled to produce a 266-nm laser beam. The 1064 nm and 532 nm components of the beam will be separated into a beam dump while the 266-nm beam is sent to the test section. The beam is formed into a laser sheet approximately 2 inches high and 500 micron thick by a series of cylindrical lenses. The beam then passes through a 4"x4" fused silica window into the duct. The beam traverses the model cross section of concern and passes through the 4"x4" window on the other side.

Working Fluids Selection

An iterative design process was used to determine which gases should be used as simulants for the nozzle flows. A spreadsheet, using quasi-1D nozzle flow equations,[9] was used to calculate the Mc_{rt} for a variety of gases and nozzle conditions. The turbine simulant has to be heated to make sure the acetone would remain vaporized in the turbine flow. This greatly affected the ability of the gases to achieve $Mc_{rt} = 0.6$ and stressed the power requirement of the rocket simulant heater.

The first gases explored were air and nitrogen as rocket and turbine simulants respectively. The air/nitrogen combination could not reach $Mc_{rt} = 0.6$, even when the exit temperature of the turbine nozzle was below the condensation point of acetone. Helium was also considered for the turbine simulant, but the combination could not achieve $Mc_{rt} = 0.6$ due to helium's higher γ and lower molecular weight. A combination using helium as rocket simulant and air or nitrogen as turbine simulant could reach $Mc_{rt} = 0.6$; however, helium is an expensive gas that requires special piping and sealing considerations to prevent leaks. Carbon dioxide was examined as a simulant for the turbine nozzle. Carbon dioxide has a lower γ and a higher molecular weight than air (the rocket simulant) which made it a better turbine simulant than nitrogen.

An air compressor will pump a 500-ft^3 tank to 1100 psi. This tank will be blown down to 925 psi, supplying the model with high-pressure air as the rocket simulant. Fig. 2 shows the achievable Mc_{rt} of this air supply tank with and without the use of a 260-kW heater. Since the carbon dioxide exiting the turbine nozzle must remain above the condensation temperature of acetone, the air will be heated to over 600° R with the 260-kW heater in order to reach a Mc_{rt} close to 0.6.

Model Design

The baseline model design was chosen at one-sixth geometric scale to facilitate comparison of cold flow data with subscale motor firings. A configuration with two rocket nozzles and one turbine nozzle was elected in order to minimize the mass flow rate requirements. The simulants will be air (rocket) and carbon dioxide (turbine). The rocket nozzle will have a chamber temperature of at least 600° R, chamber pressure of 600 psi, mass flow rate of 4.0 lbm/sec, and an area ratio of 4.5. The rocket nozzles are designed to exit at atmospheric pressure (14.7 psi). The turbine nozzle will have a chamber temperature of 760° R, chamber pressure of 90 psi, mass flow rate of 0.09 lbm/sec, and an area ratio of 1.126. The turbine nozzle was designed to have an exit pressure greater than the rocket nozzle wall pressure at their point of intersection to facilitate the vertical expansion and mixing of the turbine exhaust gas into the rocket exhaust gas. The exit temperature of the turbine exhaust must be greater than 590° R to avoid condensation of acetone in the flow within the viewing area.

Figure 3 shows the side and rear views of the stainless steel model. The strut is only 1 inch wide and 6.5 inches tall. The model will be tested in a duct with internal dimensions of 4 inches high and 3.4 inches wide. The small duct width will create measurable air entrainment. The primary rocket nozzles have circular chambers and throats which transition to approximately 0.83 x 0.83-inch square exits as in the full-scale version. The turbine nozzle is a rectangular duct that is 0.49 x 0.09 inches at the exit. The turbine exhaust nozzle intersects the wall of the rocket nozzles about 0.23 inches before the rocket nozzle exit plane. These nozzles have the same divergence angles currently envisioned for full-scale models. Three more models will offer variations from this baseline design.

The effect of the ingested flow upon the turbine/rocket flow mixing is not understood at this time. The lateral rate of spreading of the turbine exhaust stream as a function of distance downstream is expected to provide a measure of this effect.

Test Plan

The first item in the test program will be verification of the diagnostic method. Acetone will be seeded in the turbine simulant at increasing levels to determine when and if it will condense. The laser and camera will be positioned and tested. Pressure measurements will be carefully taken to determine if the system reaches a steady state, and Pitot probes will sample the nozzle exhaust to verify predicted nozzle exit conditions. Pitot probes will also be used to sample the ingested airflow to understand its behavior and possible impact on mixing. Temperature measurements will also be made in the chamber to estimate delivered Mc_{rt}. Once the check out is complete, the primary testing will begin. The rocket chamber temperature will be varied between 600 and 700° R with the 260-kW air heater. This will change the convective Mach number from around 0.5 to a little over 0.6. Acetone-based PLIF images will be taken for a least three convective Mach numbers to see how the mixing varies with Mc_{rt}. Data will be taken at the rocket nozzle exit plane, and at L/D (distance from the exit plane/nozzle exit diameter) of 9 and 18. It is expected that complete mixing will be achieved by an L/D of 18. The stations selected provide an opportunity to observe the mixing process of the turbine and rocket exhaust plumes from the exit plane to where complete mixing is envisioned. At least two tests at each measurement location and Mc_{rt} will be taken to enable statistical analysis. There is a maximum of four models planned for testing including the baseline model.

Conclusions

This experiment meets the established requirements: a convective Mach number at 0.6 is achievable and the model's scale is not smaller than one-sixth. The experiment uses heated air as the rocket exhaust simulant and heated carbon dioxide as the turbine simulant. Acetone-based PLIF will be used to visualize and quantitatively evaluate the rocket and turbine exhaust flows. The test results will be used to complement hot fire testing.

Acknowledgments

NASA Marshall Space Flight Center is providing funding and technical support for this mixing experiment under Cooperative Agreement Number NCC8-123. Aerojet has assisted with the planning of the experiment, and Rapid Tech Engineering is constructing the test model.

References

[1]Bulman, M. and Siebenhaar, A., "The Strutjet Engine: Exploding the Myths Surrounding High Speed Airbreathing Propulsion," AIAA Paper 95-2475, July 1995.

[2]Bulman, M., Private Communication, Aerojet, September 6, 1996.

[3]Papamoschou, D. and Roshko, A., "The Compressible Turbulent Shear Layer: An Experimental Study," *Journal of Fluid Mechanics*, Vol. 197, 1988, pp. 453-477.

[4]Papamoschou, D., "Structure of the Compressible Turbulent Shear Layer," *AIAA Journal*, Vol. 29, 1991, pp. 680-1.

[5]Bunyajitradulya, A. and Papamoschou, D., "Acetone PLIF Imaging of Turbulent Shear Layer Structure at High Convective Mach Number," AIAA Paper 94-0617.

[6]Eaton, A. R., et al., "Development of a Full-Field Planar Mie Scattering Technique for Evaluating Swirling Mixers," *Experiments in Fluids*, Vol. 21, 1996, pp. 325-330.

[7]Clemens, N. T. and Mungal, M. G., "A Planar Mie Scattering Technique for Visualizing Supersonic Mixing Flows," *Experiments in Fluids*, Vol. 11, 1991, pp. 175-185.

[8]Lozano, A., Yip, B., and Hanson, R. K., "Acetone: a Tracer for Concentration Measurements in Gaseous Flows by Planar Laser-Induced Fluorescence," *Experiments in Fluids*, Vol. 13, 1992, pp. 369-376.

[9]Sutton, G., *Rocket Propulsion Elements*, 6th ed., Wiley, New York, 1992.

Figure Captions

Fig. 1 Rocket and turbine exhaust mixing in the Strutjet.[2]

Fig. 2 Achievable convective Mach numbers.

Fig. 3 Side and rear views of the cold flow test model.

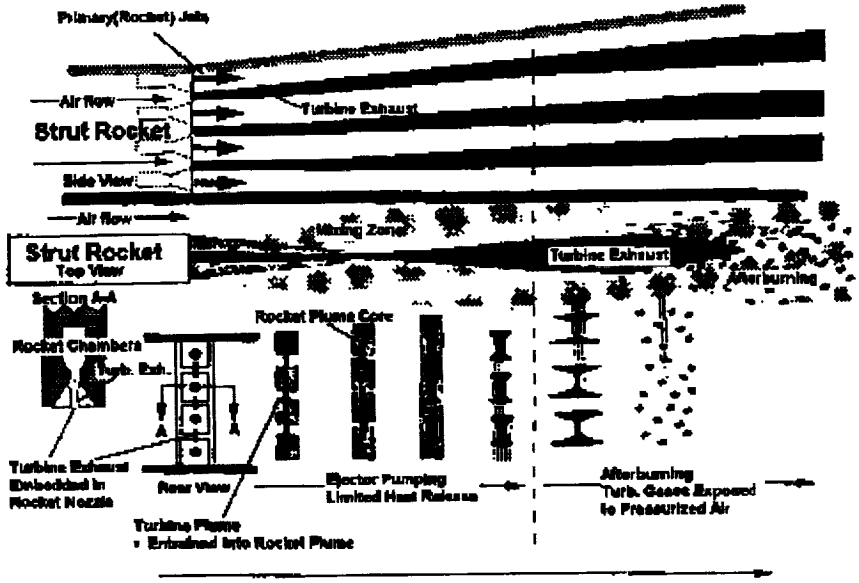
Primary(Rocket) Jets
Air flow
Strut Rocket
Side View
Air flow
Turbine Exhaust
Strut Rocket
Top View
Mixing Zone
Turbine Exhaust
Afterburning
Section A-A
Rocket Chambers
Turb. Exh.
Rocket Plume Core
A
A
Turbine Exhaust
Embedded in
Rocket Nozzle
Rear View
Ejector Pumping
Limited Heat Release
Afterburning
Turb. Gases Exposed
to Pressurized Air
Turbine Plume
Entrained into Rocket Plume
Distance From Rocket Exit Plane

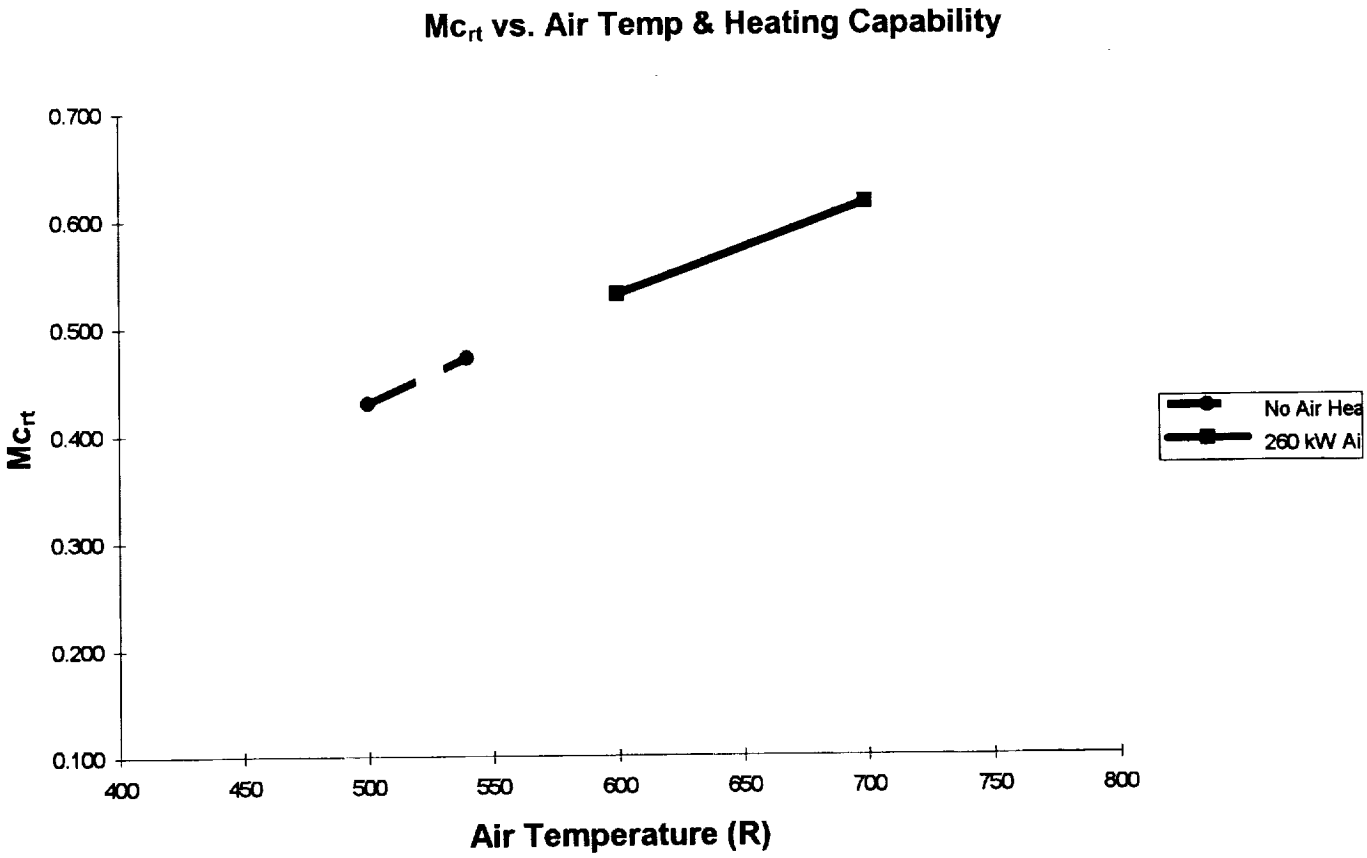
Mc$_{rt}$ vs. Air Temp & Heating Capability
0.700
0.600
0.500
0.400
0.300
0.200
0.100
Mc$_{rt}$
400
450
500
550
600
650
700
750
800
Air Temperature (R)
No Air Hea
260 kW Ai

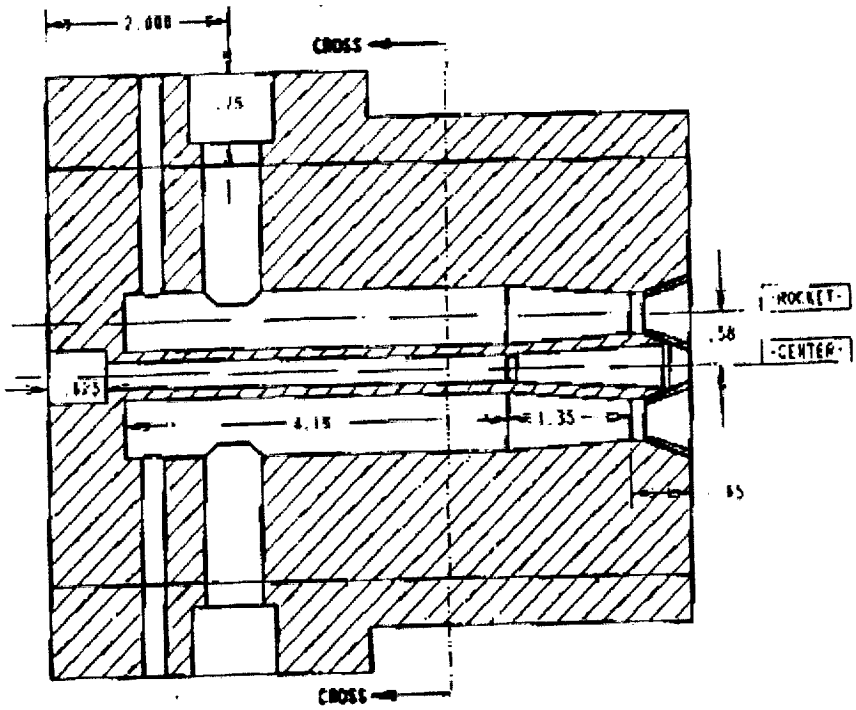
2.000
CROSS
.15
.58
ROCKET
CENTER
.625
4.15
1.35
.85
CROSS

Mixing of Supersonic Jets in a RBCC Strutjet Propulsion System

S.Muller*, Dr. Clark.W.Hawk†, prof. dr. ir. P.G.Bakker**
D.Parkinson‡ and M.Turner‡
University of Alabama in Huntsville
Huntsville, AL 35899

Abstract

The Strutjet approach to Rocket Based Combined Cycle (RBCC) propulsion depends upon fuel-rich flows from the rocket nozzles and turbine exhaust products mixing with the ingested air for successful operation in the ramjet and scramjet modes. It is desirable to delay this mixing process in the air-augmented mode of operation present during take-off and low speed flight.

A scale model of the Strutjet device was built and tested to investigate the mixing of the streams as a function of distance from the Strut exit plane in simulated sea level take-off conditions. The Planar Laser Induced Fluorescence (PLIF) diagnostic method was employed to observe the mixing of the turbine exhaust gas with the gases from both the primary rockets and the ingested air. The ratio of the pressure in the turbine exhaust to that in the rocket nozzle wall at the point of their intersection was the independent variable in these experiments. Tests were accomplished at values of 1.0 (the original design point), 1.5 and 2.0 for this parameter and images of the degree of mixing taken at 8 locations downstream of the nozzle exit plane. The results illustrate the development of the mixing zone from the exit plane of the strut to a distance of about 18 equivalent rocket nozzle exit diameters downstream (18"). These images show the mixing to be confined until a short distance downstream of the nozzle for a single nozzle geometry set. The lateral expansion is more pronounced at pressure ratios of 1.0 and 1.5 indicating that mixing with the ingested air flow would be likely to begin at an L/D of approximately 1 downstream of the nozzle exit plane. Of the pressure ratios tested in this research, a value of 2.0 delays the mixing until 2" downstream and is the best value at the operating conditions considered.

Introduction

Even though space travel is not as new and extraordinary as it used to be just 2 decades ago, it is still a very expensive activity. The next step in the efforts to reduce the costs is to make the Single Stage To Orbit (SSTO) concept a reality. It is envisioned that this would lead to 'airline'-like operation of the launch vehicle. The development of airbreathing propulsion concepts like Rocket Based Combined Cycle (RBCC) is seen as a key issue in the development of SSTO. The research discussed in this paper addresses the Strutjet configuration applied to an RBCC.

Specifically, the research focused on the mixing behavior of rocket and turbine exhaust jets in the RBCC Strutjet concept during a simulated sea level take-off condition. The Strutjet propulsion concept is designed to operate in four different modes: ducted rocket or air augmented

---

* Student at the Faculty of Aerospace Engineering, Delft University of Technology, The Netherlands
† Professor of Mechanical and Aerospace Engineering at the University of Alabama in Huntsville and Director of the Propulsion Research Center
** Professor at the Faculty of Aerospace Engineering, Delft University of Technology, The Netherlands
‡ Student at the University of Alabama in Huntsville
‡ Student at the University of Alabama in Huntsville

mode, ramjet mode, scramjet mode and a pure rocket mode (Ref 1). A variable inlet directs the air into the flow channel where struts containing rocket motors are located. This inlet can be adjusted to provide the compression of the ingested air needed in the (sc)ramjet mode. On the aft side of the engine, a variable nozzle expands the combustion gases generating thrust. The rocket motors have turbopumps driven by fuel-rich running gas generators (GG) that also exhaust at the downstream side of the struts.

In the air-augmented rocket mode that is of interest here, the mixing of the fuel-rich turbine exhaust with the ingested air should be delayed to prevent thermal choking in the expansion part of the engine. The nozzle layout investigated in this research was designed to achieve this by injecting the turbine exhaust between the rocket plumes in order to shield the fuel-rich exhaust from the ingested air and delay the heat release. (Figure 1) This configuration should promote mixing in the vertical direction (among the turbine and rocket exhausts) before they mix with the ingested air. The goal of this research was to determine the effectiveness of the chosen geometry in delaying mixing with the ingested air in the air-augmented mode of operation.

Experimental Setup

Flow section

This research is done with a $1/6^{th}$-scale model of one strut equipped with two rocket exhausts flowing heated air and one turbine exhaust in between them, flowing heated CO_2. The area ratio of the rocket nozzles is 4.65 and of the turbine nozzle 1.184. The turbine exhaust plane is located upstream of the rocket exhaust plane. (Figure 2). This means that the flow from the turbine comes into contact with the rocket flow upstream of the rocket nozzle exit plane. At this location, the area ratio of the rocket nozzle is 2.99. The design chamber pressures were chosen to have the turbine exhaust come into contact with the flow in the rocket at the same local pressure. In this research, we also tested the influence of the pressure ratio ($p_{turbine}/p_{rocket}$) of the exhausts at the point of contact, performing the measurements at three values of the ratio. These were 1.0, 1.5 and 2.0.

The model was placed in a rectangular duct (about 4" x 4" cross section) with an aluminium top and bottom and transparent sidewalls. (Figure 3). The sidewalls are modular with interchangeable sections to allow easy access to the inside of the duct and direct observation of the flow. The duct has a two-dimensional bellmouth inlet made out of sheet metal open to the atmosphere providing a smooth ingested airflow. It is oriented with the longest dimension parallel to the strut. The rear side of the duct exhausts into a 10-inch diameter sheet metal pipe of which the front side is open. This allows extra air to be drawn in the exhaust slowing down the jet exiting from the duct. The pipe discharges the flow into free air. (Figure 6) (Ref. 6)

In order to achieve the same mixing behavior in the scaled experiment as in the real size system, a similarity parameter of convective Mach Number was used. Papamoschou and Roshko (Ref. 2) experimentally found this similarity parameter for supersonic shear layer growth rates. (Ref. 5) The definition below assumes: (1) similar specific heat ratios, (2) equal static pressures at the shear layer and (3) steady flow conditions.

$$M_{c_1} = \frac{U_1 - U_c}{a_1} \approx \frac{U_c - U_2}{a_2} = M_{c_2}$$

in which U_c is defined by:

$$U_c \approx \frac{a_2 U_1 + a_1 U_2}{a_1 + a_2}$$

As can be observed from the definition, the convective Mach number can be calculated by using either one of the flows as reference. The two methods are exactly equal in the case that both flows have the same specific heat ratios. U_c, the convective velocity, is a speed of sound weighted average of the two flow velocities and represents the velocity of the dominant waves and structures present in turbulent flow.

A convective Mach number of 0.6 was chosen for the experiments as representative of the full-scale engine. The convective Mach number was calculated for each test run and was taken at the point where the two flows come into contact with each other at their point of intersection.

The diagnostics technique that was chosen, PLIF, used acetone as the seedant in the turbine flow. The CO_2 carrier gas needed to be heated to 760°R stagnation temperature in order to prevent acetone from condensing in the nozzle, To maintain the convective Mach number at 0.6, the rocket nozzle flow and the turbine flow should have the same stagnation temperature.

The two rocket nozzles received heated air from two tanks with a combined volume of 524 cubic feet. These tanks were pressurized up to 2500 psi with a 6000 psi air compressor, which delivers very clean and dry air (dew point –65 °F). These tanks supply air to a 240 kW electric heater, which was used to heat the air to 760°R at the model. This air supply system (Figure 4) can deliver air with a total pressure of up to 750 psi and mass flow of about 4 lbm/s. The total pressure of the air was regulated by a control valve using a feedback pressure measurement taken in the simulated combustion chamber of the model and can be set at any value.

The turbine nozzle was supplied with CO_2 stored in 4 K-bottles. The CO_2 was expanded in two pressure regulators in series from about 1000 psi to the 90 psi needed at the model. A water bath heater was used to heat up the CO_2 coming out of the bottles and after each stage of pressure regulation. Then a 12 kW electric heater is used to heat up the CO_2 to the 760°R needed at the model. This system supplies a 0.1 lbm/s flow of CO_2. (Figure 5.)

The acetone seeding system sprayed laboratory grade acetone through a nozzle into the CO_2 flow as it enters a large mixing chamber situated downstream of the 12 kW electric heater. The spray nozzle was fed out of a nitrogen pressurized acetone container. This container was filled with the required amount of acetone and then brought to, and maintained at, a pressure of about 325 psi. This maintained the pressure drop over the spray nozzle at a minimum of 225 psi, which was required to keep the seeding at a constant molar fraction of 11%.

Instrumentation

To monitor the operating conditions of the experiment, the systems supplying the gases to the model and the duct inlet were instrumented. The instruments also allowed on-line monitoring of the gas supply systems during the testing. The measurements were recorded as each test proceeds. The locations of the measurements in the gas supply systems are shown in Figures 4 and 5. The instrumentation locations in the duct inlet are shown in Figure 6.

The pressure and temperature in all three nozzles are measured in the simulated 'combustion' chambers and recorded. The pressure measurement in the rocket chamber is also used to feedback the controller of the regulating valve in the air supply system. Further on, this data was used to determine the convective Mach number at which the testing was performed.

In the air supply system, the temperature at the exit of the heater was measured to provide feedback for the heater controller. This measurement was not recorded. At the point where the air

from the storage enters the heater a glue-on thermocouple is mounted to monitor the behavior of the heater.

In the CO_2 system, the pressure and temperature is measured at the exit of the waterbath-heater, at the entrance and at the exit of the acetone seeder. (Figure 5). This data allows the monitoring of the CO_2/Acetone system.

In the inlet of the duct, the ingested air pressure was monitored with a separate pitot and static pressure tube at the point where the cross section just reached the dimensions of the duct. A pitot-static tube in the fairing in front of the model, hooked up to two separate transducers, provides a verification possibility for the measurement in the inlet. A static pressure port was drilled in the sidewall in the gap between the sidewall and the strut model. (Figure 6). These inlet pressure measurements were used to verify that the conditions of the ingested air are identical from test to test.

Diagnostics

As said before, the PLIF diagnostic method was used to visualize the gas flows. PLIF is based on the ability to make a substance fluoresce with laser radiation and imaging it with a camera. In these experiments, the turbine flow was seeded with laboratory grade acetone as described in the previous paragraph. This acetone was then excited with UV radiation with a wavelength of 266 nm. This UV radiation was provided by a frequency quadrupled Spectra-Physics Quanta-Ray GCR290 Nd:YAG laser, emitting pulses of 10 ns at a rate of 10 Hz. The 1064 nm IR and the 532 nm second harmonic green radiation resulting from the doubling of the laser output are separated from the UV and sent to a beam dump. The UV radiation is made into a laser sheet 3.5" high and about 500 microns thick by means of a convex and a cylindrical lens and guided to the test location. This location can be moved along the duct by moving the last prism and the two lenses. (Figure 7)

Because plexiglas absorbs UV radiation, special sections of the duct sidewall were made with cutouts that hold a fused silica window (3.5" x 3.5"). These special sections can be mounted in the sidewall at different locations around the nozzle exit plane, 9" downstream and 18" downstream of the nozzle exit plane. This window allows the UV sheet to enter the test section. The acetone vapor is then excited and fluoresces emitting broadband radiation at wavelengths between 300 nm and 700 nm. The fluorescent signal was collected over a bandwidth of 300-495 nm to eliminate interference from scattered 266 nm and 532 nm laser light. Ref. 4 shows this range of wavelengths to account for about 80 % of the fluorescence radiation energy ensuring that a sufficient amount of signal is available for collection. On the other side of the duct one long piece of plexiglas was mounted to allow an unobstructed view for the camera. This sidewall will absorb the remainder of the UV radiation, while a Visible Short Pass (VSP) Filter in front of the camera absorbs light with a wavelength over 495 nm.

The signal was collected by a Princeton Instruments ICCD camera. The setup of the camera is illustrated in Figure 8. For each of the three window locations (exit plane, 9" and 18") the camera was mounted on the table with the viewing axis at an angle of 30° to the centerline of the duct. The laser sheet was moved axially within the silica window area to collect data at different locations. The angle at which the fluorescence was viewed is 30 ±2.5°. (Depending on the location of the laser sheet)

Acetone fluorescence has a lifetime of less than 4 nanoseconds. Acetone also phosphoresces at wavelengths similar to the fluorescence, albeit at a much greater lifetime of about 200 microseconds. The phosphorescence interference was rendered negligible by gating the intensified camera around the laser pulse (10 ns) at 13 nanoseconds. This also eliminated interference from surrounding light sources.

Experimentation

Tests were performed for the three pressure ratios (1.0, 1.5 and 2.0) between the rocket and turbine nozzles. With the chamber pressure of the turbine nozzle maintained at 98 ± 5 psia, the rocket chamber pressures were set to 550 psia, 366 psia and 275 psia respectively to achieve these pressure ratios. The pressure at the point of intersection for these operating conditions yielded 26.2 ± 1.3 psia in the turbine exhaust and 26.2 psia, 17.4 psia and 13.1 psia respectively in the rocket nozzle.

Images were recorded at 8 locations from the exit plane of the rocket nozzles and downstream, bringing the total number of tests to 24. All locations are indicated as a distance from the exit plane of the rocket nozzles as shown in Table 1.

Table 1: Test Matrix

	Laser Beam Location							
Window Position	Exit plane					9"		18"
Press. Ratio	Exit	0.5"	1"	1.5"	2"	7"	10.25"	18"
2.0	X	X	X	X	X	X	X	X
1.5	X	X	X	X	X	X	X	X
1.0	X	X	X	X	X	X	X	X

All the tests were performed at a convective Mach number of 0.6. To achieve this, the temperatures of the gases were maintained, as close as the heaters would allow, to the 760°R needed. The actual convective Mach number was calculated from the temperatures measured in the nozzle chambers during the test.

The laser and optics were set to produce the laser sheet with an energy between 80 and 85 mJ in the UV (266 nm) entering the test section. The laser energy was monitored and maintained at this energy level for all tests.

The camera was synchronized with the laser pulse and operated in gated mode. It was also cooled to reduce background noise and therefore needed to be purged with dry nitrogen to prevent condensation inside the camera. The intensifier has a controllable gain, which can be set to any value between 0 and 10. The camera settings, that were the same for all tests, were:

- Gate width: 13 ns
- Gain Setting: 9.0
- Intensifier temperature: -28° C

The camera used a Nikkor 60 mm / f2.8 lens, set at the f-stops indicated in Table 2

Table 2: Lens Settings

	Laser Beam Location							
Press. Ratio	Exit	0.5"	1"	1.5"	2"	7"	10.25"	18"
f-stop	5.6	5.6	5.6	5.6	5.6	4.0	4.0	4.0

A test run was performed by ramping up the air supply system by inputting the desired pressure as setpoint in the controller of the regulating valve. It took about 20 to 30 seconds for the pressure to reach the setpoint. When the desired test conditions in the chambers of the nozzles reached steady state, the camera was started and 10 pictures were taken in about 30 seconds. Right after starting the camera, the seeding of the acetone was started. It took about 4 seconds to reach steady seeding at the model. This means that the first 2 images will not have any

fluorescence on them. One of these images was used to subtract from the later pictures, where full fluorescence was recorded, to remove any light that was not due to fluorescence.

To enable the scaling of the images to correct for the difference in distance to the camera, an image of a piece of cardboard, with the outline of the nozzles on it, was taken in the same plane as the laser sheet. Horizontal and vertical reference lengths were measured in each of those images to determine the scaling ratios, which were used for correction of the fluorescence images.

Image processing and results

The fluorescent signal

Fluorescence from acetone for weak excitation can be modeled by the following relationship showing the wavelength and temperature dependencies (Ref. 3):

$$S_f(\lambda,T) = \eta_{opt}\,(E / (hc/\lambda))\, dV_c\, n_{abs}(T)\, \sigma(\lambda,T)\, \phi(\lambda,T)$$

Where S_f is the intensity of the fluorescence, η_{opt} is the overall efficiency of the collection optics, E is the laser fluence (J/cm^2), (hc/λ) is the energy (J) of a photon at excitation wavelength λ and dV_c is the collection volume (cm^3). The temperature dependent quantities are n_{abs}, the number density of absorbing molecules (cm^{-3}); σ, the molecular absorption cross section of the tracer (cm^2) and ϕ, the fluorescence quantum yield.

Since the optical setup is the same for all tests performed, the overall efficiency of the collection optics, n_{opt}, was assumed to be constant. E, the laser fluence was also assumed to be a constant, because the laser energy was monitored and kept at the same level for all tests and the dimensions of the laser sheet entering the test section were constant. (hc/λ), the energy of the photons, depends only on the wavelength of the laser light and is therefore also constant. The term $\sigma(\lambda,T)\ \phi(\lambda,T)$ was defined as $S_f^*(\lambda,T)$ in Ref. 3 and has a relatively small dependency on temperature for the range expected to occur in the experiment. The maximum variation is about 10% for the temperature range (300 K - 450 K) of the experiment. The term $dV_c\, n_{abs}$ is equal to the number of tracer molecules hit by the laser. Because the laser sheet had the same dimensions for all tests, this term is proportional to the density of the acetone in the CO_2 and because the molar fraction of the seeding is constant, the term is also proportional to the density of the entire turbine flow.

The above implies that if there is a variation greater than 10% in the fluorescence signal, this must be due to a variation in the density of the turbine flow. This density change can be caused by an event like a shock or expansion wave, which does not necessarily mean that mixing has taken place. Therefore, the images were normalized to the total fluorescence signal of the picture. This provides a picture that shows the percentage of molecules hit by the laser within each pixel of the image. High values in an image will then indicate the presence of a concentrated core flow, while low values will show that the turbine flow is spread out.

Processing of the images

From each test run, one image was retained that was most representative of the run. The software from Princeton Instruments (WinView 1.6.2) used to operate the camera was also used for further processing of the images. After subtraction to remove the background reflections the images were normalized to the total fluorescence signal. To further reduce the influence of the background, all the negative values in the image, caused by small differences between the background image and the background of the fluorescence image, were first set to 0. The total

signal was then determined by adding the values of all the pixels with a value of over 10% of the maximum value in the image. The threshold was set at 10% to minimize the contribution of the background to the total.

Each pixel of an image covers an area, which is dependent on the distance from the camera. To correct for this effect, the value of the pixels was also divided by the surface scaling factor that was determined. The surface scaling factor is the result of the multiplication of the horizontal and vertical scaling factors that were measured as described in the Experimentation paragraph. See Table 3.

Table 3: Scaling factors.

Location (inches)	Dimensions (pixels)		Scaling Factors		
	Horizontal	Vertical	Horizontal	Vertical	Surface
Exit	190	75	1	1	1
0.5"	204	83	0.9314	0.9036	0.8416
1"	202	97	0.9406	0.7732	0.7273
1.5"	213	96	0.8920	0.7813	0.6969
2"	212	95	0.8962	0.7895	0.7075
7"	191	81	0.9948	0.9259	0.9211
10.25"	228	101	0.8333	0.7426	0.6188

Results

The resulting images can be seen in Figure 9. To enable comparison of the size of the turbine flow, these images have also been resized to the same scale. Top to bottom is going downstream from the nozzle exit plane. Left to right are the pressure ratios, decreasing from 2.0 to 1.0. In the Figure, the pixels have a color that represents the value of that particular pixel. The order of the colors with increasing value is: black, blue, green, orange, red and white. Please note that the figure is rotated 90° counter-clockwise as can be seen from the caption.

The images taken at a pressure ratio of 2.0 are shown in the left-hand column. At the exit plane, the turbine flow is clearly expanding into the rocket nozzles forming a shape best described by an "I". At 0.5", the turbine flow has expanded a bit in the horizontal direction. In the vertical direction it stays about the same. The "I"-shape is still very visible. At 1", the same basic shape is still there, but has spread a little horizontally. The central part of the flow is still very confined. At 1.5", this central part is still the same, but the top and bottom extremities are starting to dissolve. The turbine flow starts to separate into different parts at 2.0" and at 7" and further downstream, only a vague cloud remains.

In the middle column, the images taken at a pressure ratio of 1.5 are shown. At the exit plane, the expansion into the rocket nozzles, present at a ratio of 2.0, is less pronounced. At 0.5", the flow is clearly more confined in the vertical direction, the height of the flow is about half of that of the nozzle. This causes the center portion of the flow to be denser as is shown by the image color. Between 0.5" and 1.0", the height of the flow stayed about the same. But the flow has expanded in the horizontal direction, spreading out the core of the flow. At 1.5", the flow has spread in the vertical direction as well, virtually eliminating the core flow. At 2.0", the flow has spread more in the vertical direction and at 7" and further downstream, it has almost disappeared.

The right hand column shows the images taken at a pressure ratio of 1.0. Here, the expansion of the turbine flow into the rocket nozzles has completely disappeared as is visible in the image taken at the exit plane. At 0.5" and 1", the flow is clearly confined vertically even more than at

the pressure ratio of 1.5, the horizontal spreading is about the same. At 1.5", the core flow, having spread very much in the horizontal direction has almost disappeared. Vertically, the flow has about the same dimension as the situation at 1.5 pressure ratio. At 2" and further downstream, the turbine flow is barely visible.

Conclusion

The lower pressure ratios (1.0 and 1.5) seem to keep the turbine flow very well confined over the first inch, but also cause it to expand horizontally. This horizontal spreading causes fairly rapid mixing with the ingested air between the 1" and 2" location for these ratios, which is shown by the grainy edges on the left and right side of the core. At the 2" location, the turbine core flow has completely disappeared for the 1.0 and 1.5 pressure ratio and mixing could be considered complete.

For the 2.0 ratio, the core flow mixes in another way. First, there is some slow mixing at the edges of the core flow, which is much larger than at the other pressure ratios. Then, around the 2" location, this core flow breaks up and the parts of the core flow then mix rapidly with the surrounding gases between 2" and 7".

Although the design of the nozzles was supposed to delay mixing between the jets and the ingested airflow, the present configuration at the design conditions (pressure ratio of 1.0) seems to force the turbine exhaust to spread very rapidly. Of the pressure ratios tested in this research, it seems that a turbine exhausting at about double the pressure of the rocket jets, is the best combination for this operating mode. This delays the mixing of the turbine flow with the rocket flows the longest. At that pressure ratio (2.0) it keeps the turbine flow well confined and thereby will limit the heat release until downstream of the 2" location.

A pressure ratio higher than 2.0 could possibly delay the heat release even more. Further testing at the same facility could prove this theory.

Acknowledgments

This research was accomplished under cooperative agreement NCC8-123 with NASA/MSFC. The authors gratefully acknowledge the advice and counsel of Mr. Mike Fazah of NASA/MSFC and Dr. Larry Cohen of GenCorp Aerojet and the encouragement of Mr. Uwe Hueter of NASA/MSFC.

References

1. Siebenhaar, A. and Bulman, M.J., "The Strutjet Engine: "*The Overlooked Option For Space Launch*", Aerojet, Sacramento, CA, AIAA 95-3124, July 1995

2. Papamoschou, D. and Roshko, A., "*The Compressible Turbulent Shear Layer: An Experimental Study*", Journal of Fluid Mechanics, Vol. 197, 1998, pp. 453-477.

3. Thurber, M. C., Grisch, F., Kirby, J. K., Votsmeier. M. and Hanson, R. K., "*Measurements and modeling of acetone laser-induced fluorescence with implications for temperature-imaging diagnostics*", Applied Optics Vol. 37, No. 21, 20 July 1998, pp. 4963-4978.

4. Lozano, A., Yip, B. and Hanson, R.K., "*Acetone: a tracer for concentration measurements in gaseous flows by planar laser-induced fluorescence*", Experiments in Fluids 13, 1992, pp.369-376.

5. Spetman, D. M., Hawk, C. W. and Moser, M. D., "*Development of a Strutjet Cold-Flow Mixing Experiment*", Journal of Propulsion and Power, Volume 15, Number 1,January-February 1999, pp. 155-158.

6. Parkinson, D, Turner, M and Wagner, D, "*Mixing of Hypersonic Streams*", UAH, AIAA-99-2454, June 1999

List of figures

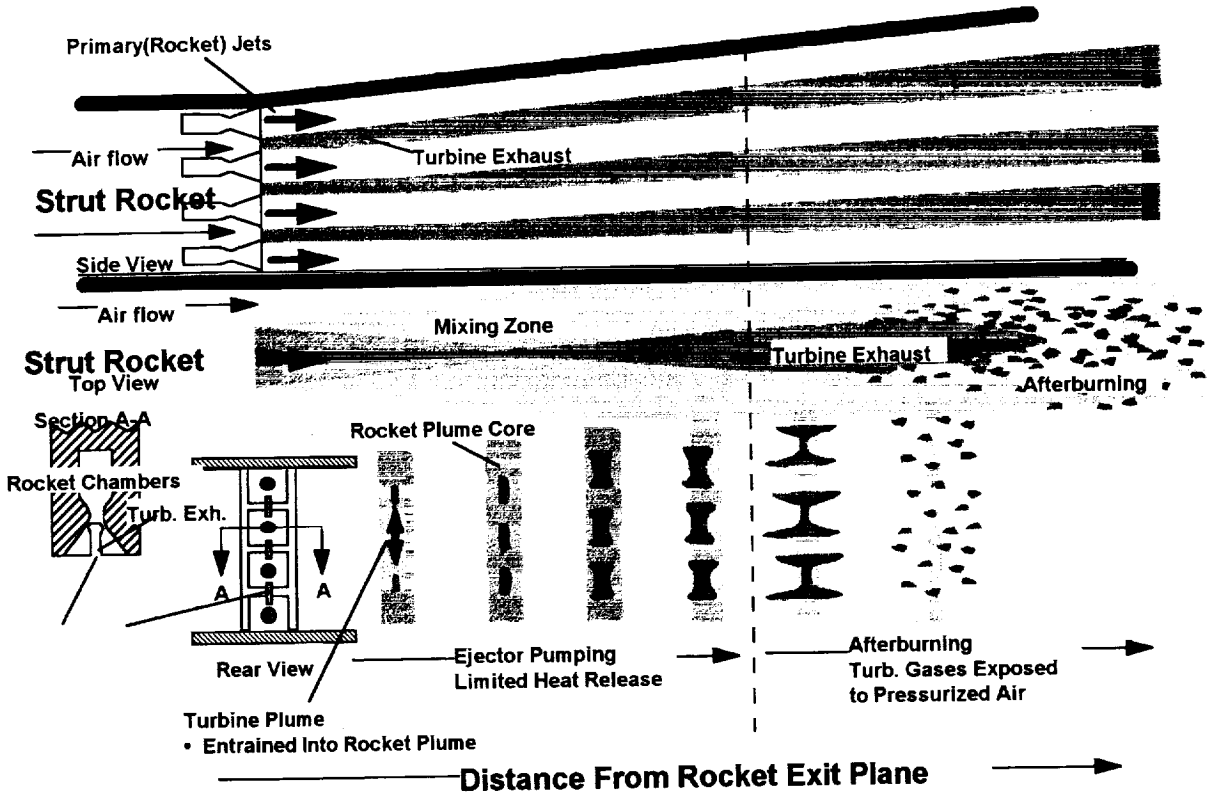

Figure 1

Figure 2

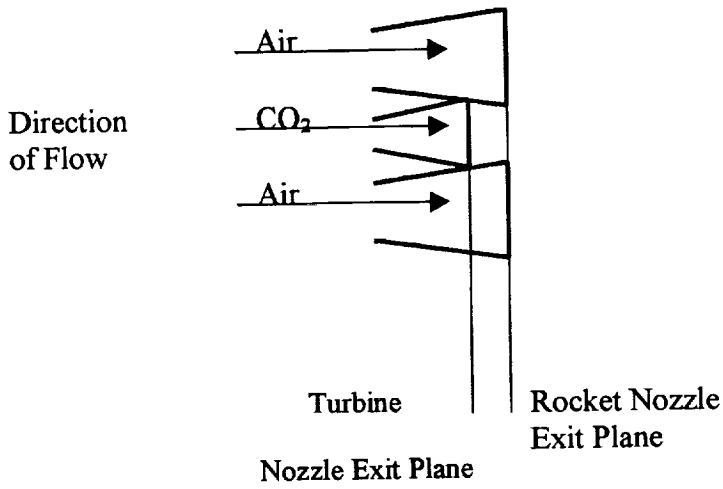

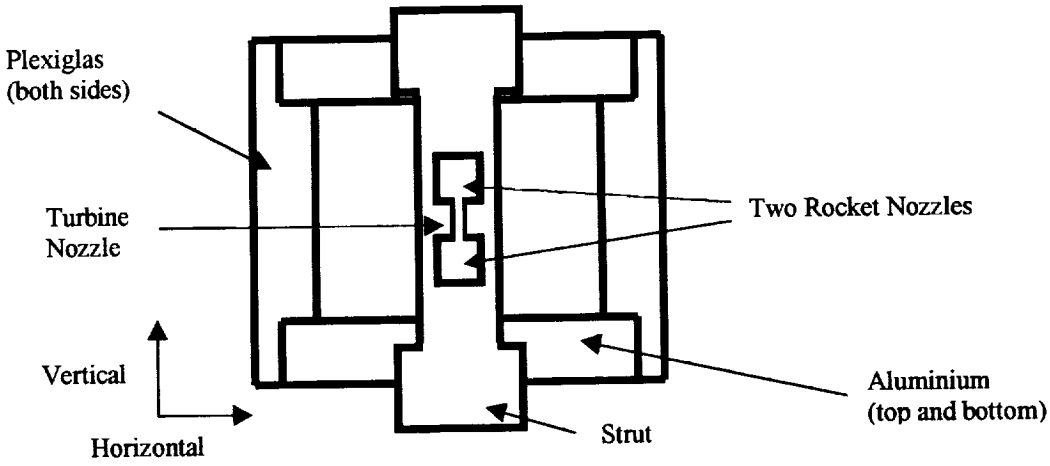

Figure 3

Figure 4

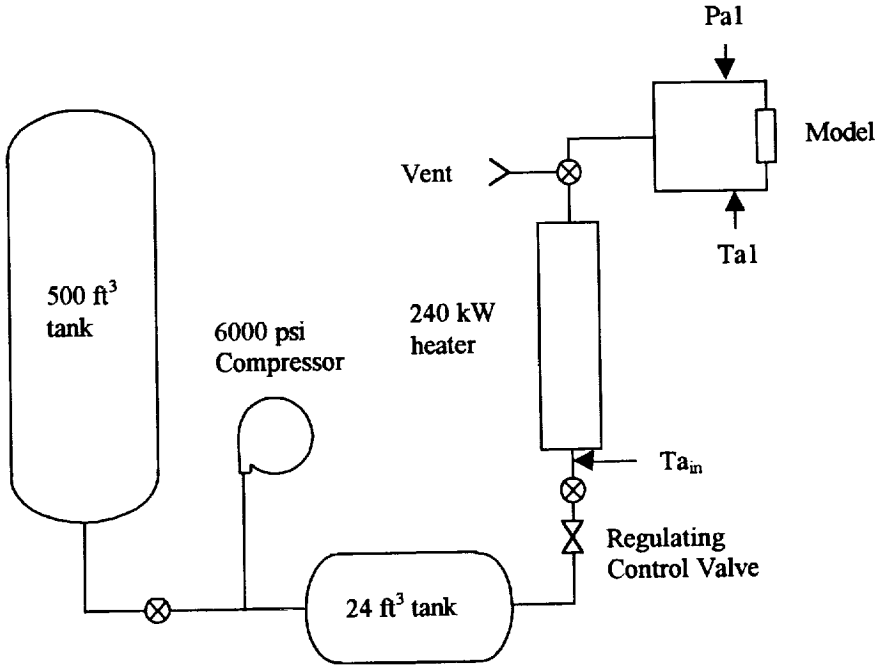

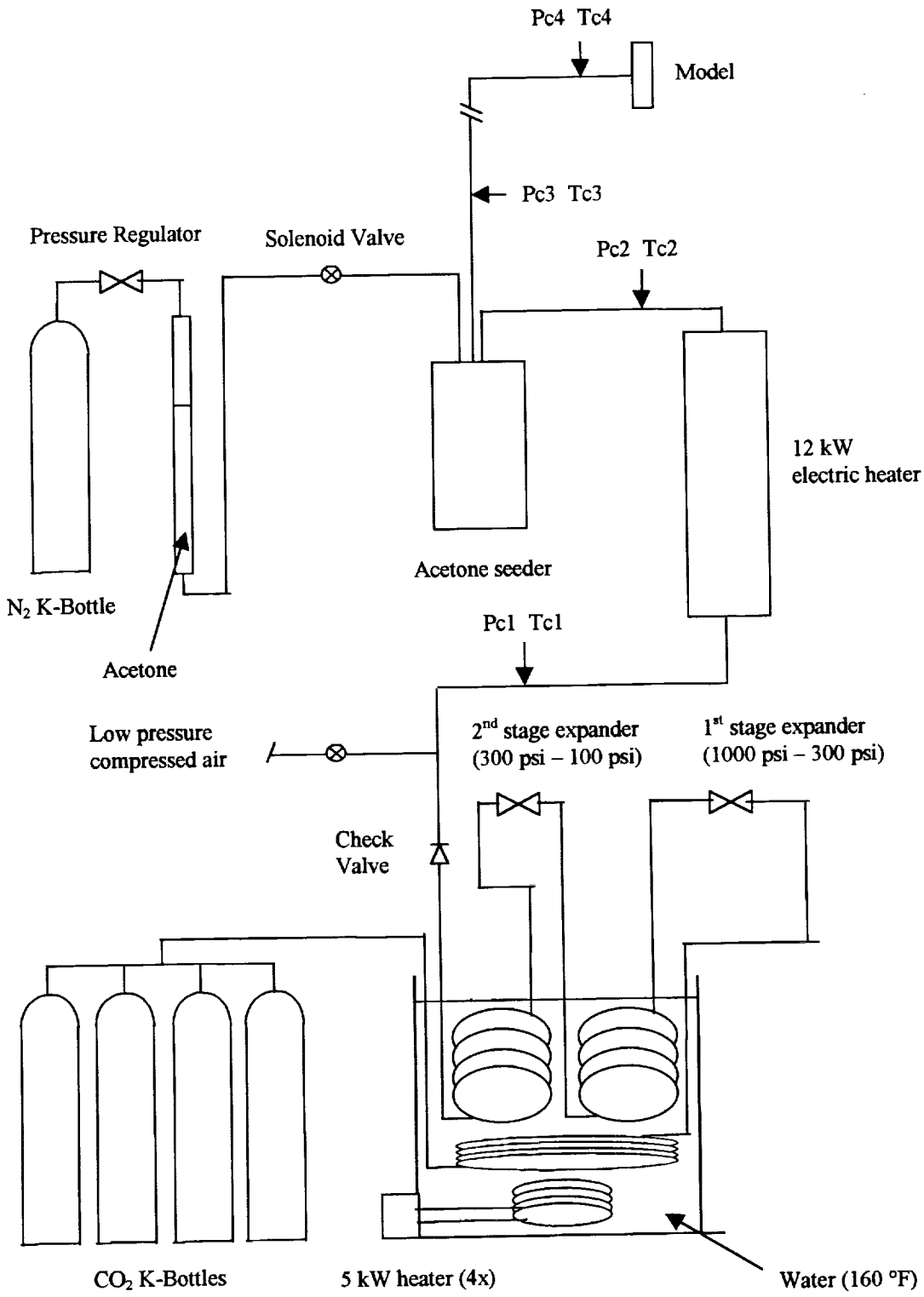
Pc4 Tc4
Model
Pc3 Tc3
Pressure Regulator
Solenoid Valve
Pc2 Tc2
12 kW
electric heater
Acetone seeder
N2 K-Bottle
Acetone
Pc1 Tc1
Low pressure
compressed air
2nd stage expander
(300 psi – 100 psi)
1st stage expander
(1000 psi – 300 psi)
Check
Valve
CO2 K-Bottles
5 kW heater (4x)
Water (160 °F)

Figure 5

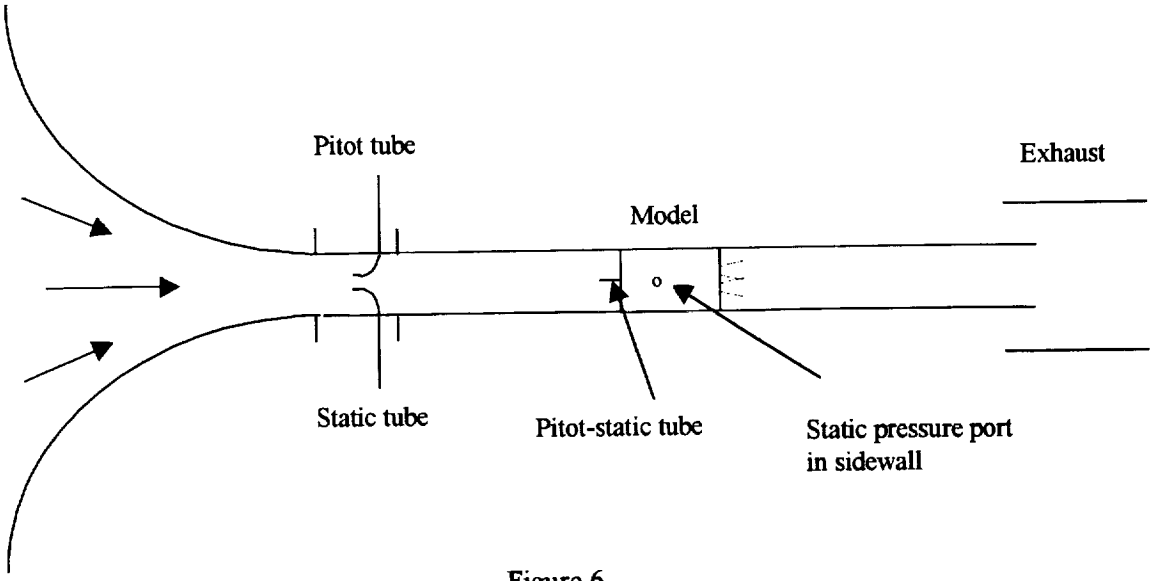

Figure 6

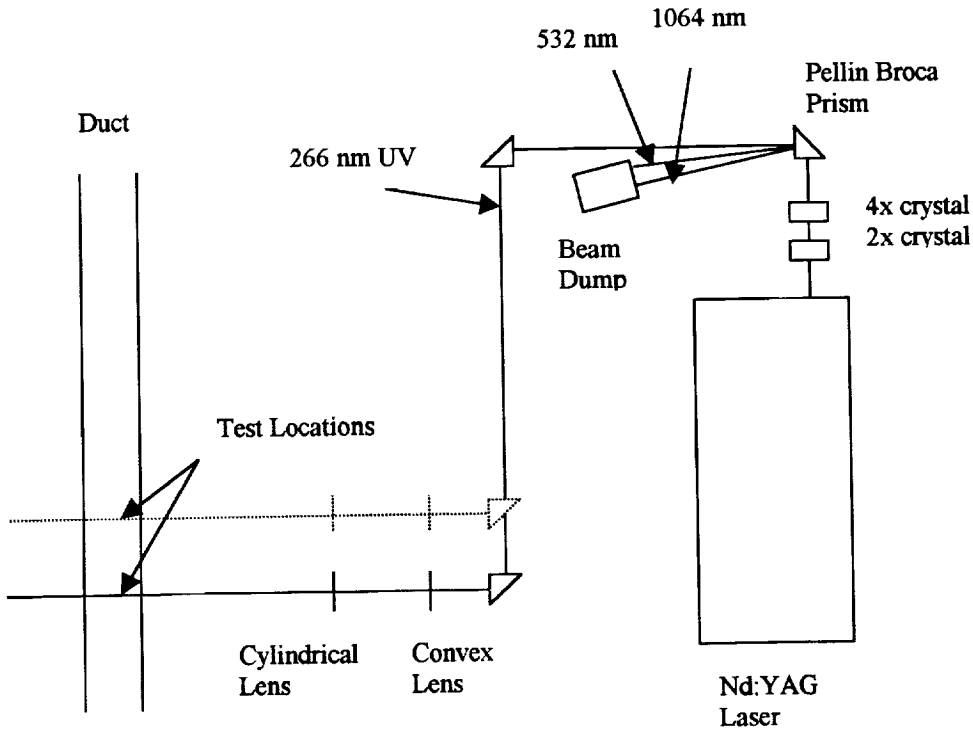

Figure 7

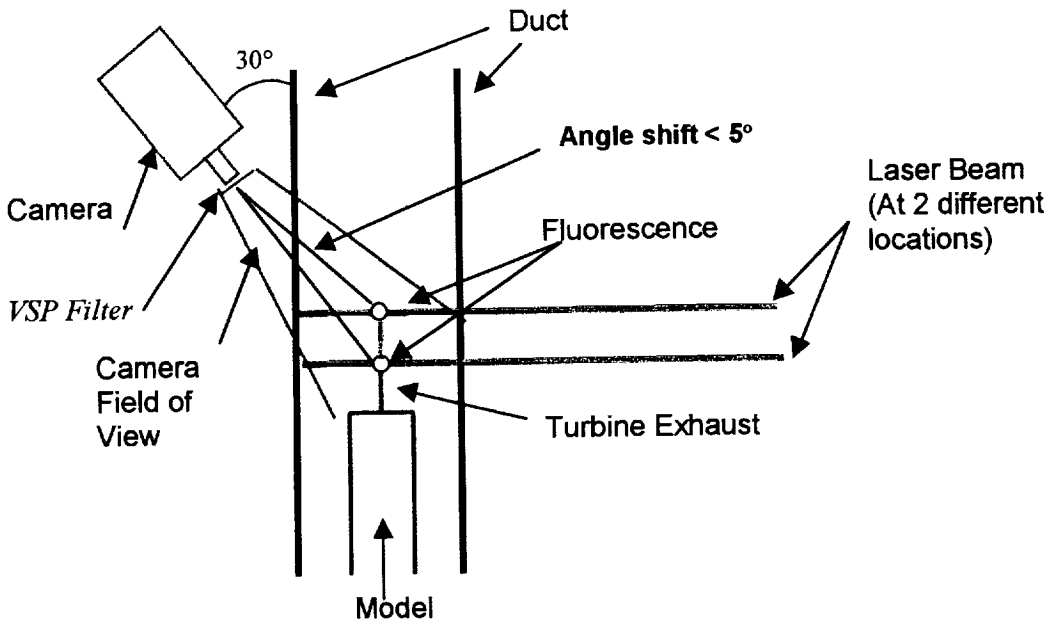
Duct
30°
Angle shift < 5°
Laser Beam
(At 2 different
locations)
Camera
Fluorescence
VSP Filter
Camera
Field of
View
Turbine Exhaust
Model

Figure 8

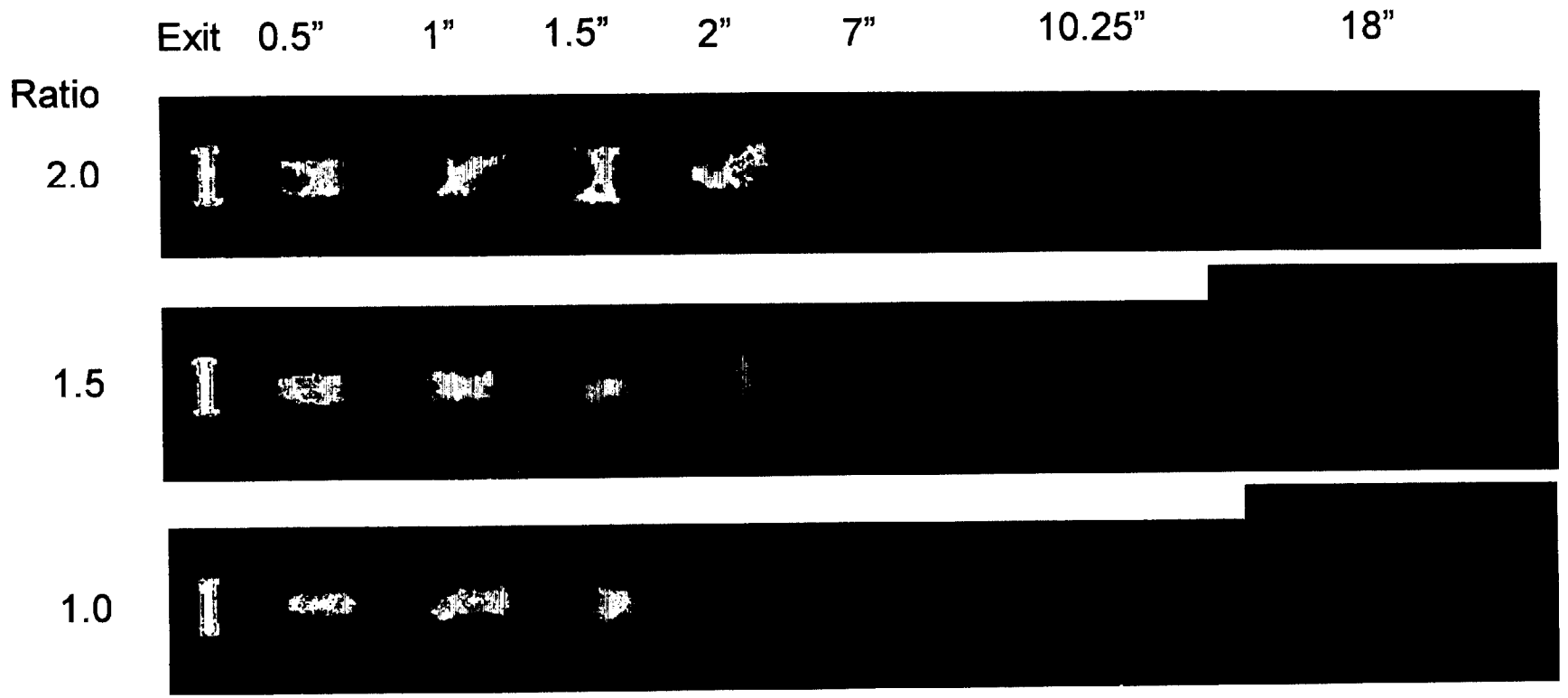

Figure 9

INVESTIGATION OF THE ROCKET INDUCED FLOW FIELD IN A RECTANGULAR DUCT

D. Brian Landrum*, Mignon Thames†, Doug Parkinson††, and Serena Gautney††
Propulsion Research Center
The University of Alabama in Huntsville
Huntsville Alabama 35899

Introduction

Ongoing research into highly reusable, Single Stage to Orbit (SSTO) vehicles seeks to attain dramatic reductions in launch costs through improvements in vehicle performance and operations. A key issue in realizing the SSTO goal is the development of air breathing propulsion concepts such as Rocket-Based Combined Cycle (RBCC). The RBCC concept is designed to obtain near optimum vehicle performance at all points in the launch trajectory by operating in four different modes: ducted rocket or air-augmented rocket mode, ramjet mode, scramjet mode, and a pure rocket mode.

The Strutjet RBCC configuration consists of a variable geometry duct with internal, vertical struts.[1,2] Each strut has several rocket and turbine exhaust nozzles embedded within it. The variable inlet directs air into the flow duct where the struts are located. The inlet is adjusted to provide compression of the ingested air as required for the ramjet and scramjet modes. A variable nozzle at the aft end of the duct expands the combustion gases generating thrust. The rocket engine propellants are supplied by turbopumps driven by fuel-rich gas generators that also exhaust at the downstream side of the struts. In the air-augmented rocket mode the mixing of the fuel-rich turbine exhausts with the ingested air should be delayed to prevent thermal choking in the expansion section of the engine. One approach is to exhaust the turbine between the rocket plumes to shield it from the ingested air and delay the heat release.

Under a NASA Marshall Space Flight Center contract, the UAH Propulsion Research Center (PRC) designed and built a cold-flow Strutjet simulation facility. A 1/6 scale model of a single strut has been built and is undergoing testing to investigate the mixing of the rocket and turbine exhausts with the ingested air. A complementary experimental program is also underway to examine the induced flow-field generated by rocket nozzles confined in a rectangular duct. Characterizing the induced flow behavior is critical to understanding and optimizing the performance of future Strutjet-based RBCC propulsion systems. The objectives for the UAH induced flow experiments are: (1) To characterize the induced airflow as a function of the primary rocket flow; (2) To determine the initial expansion rate of the rocket and turbine exhaust plumes; and (3) To assess the expansion losses in the mixer/ejector section downstream of the strut. The study includes pressure measurements at various points in the flow path and a series of pressure surveys in the duct/strut gap and downstream of the strut exit plane. This information will be used to interpret laser fluorescence data obtained on the downstream mixing of the ingested air and the rocket and turbine exhausts and to validate computational prediction codes. The data will also be used to develop analytical models to predict performance and identify key geometric parameters. The current status of the UAH research effort and important findings are summarized in this paper.

Experimental Facility

Flow Path

The UAH Strutjet simulation facility is specifically designed to investigate the mixing of the rocket nozzles and turbine exhaust products with the ingested air.[3] The primary mixing studies use air for the rockets and CO2 for the turbine. The operating conditions and gas simulants were chosen based on a desire to match the convective Mach numbers ($\approx$ 0.6) of the full-scale system in the 1/6 scale test facility.[4] However, for the induced flow study described in this paper, air was used for both rocket and turbine nozzles. The primary air supply system is shown schematically in Fig. 1. The rocket nozzles receive heated air from two tanks with a combined volume of 524 cubic feet. These tanks are pressurized up to 2500 psi with a 6000-psi air

*Associate Professor, Department of Mechanical and Aerospace Engineering. Senior Member AIAA.

†Graduate Research Assistant, Department of Mechanical and Aerospace Engineering. Student Member AIAA.

††Undergraduate Research Assistant, Department of Mechanical and Aerospace Engineering. Student Member AIAA.

compressor that delivers very clean and dry air (dew point –65 °F). The tanks supply air to a 240 kW electric heater that heats the air to 760°R at the strut model. The system can deliver air with a total pressure of up to 750 psia and a mass flow rate of about 4 lbm/s. The total pressure is regulated by a control valve using a feedback pressure measurement taken in the simulated combustion chamber of the model. Shop air for the turbine nozzle is delivered at approximately 100 psia. A 12 kW electric heater is used to heat the air up to approximately 700 °R. At this temperature an air mass flow rate of approximately 0.1 lbm/sec is delivered through the turbine nozzle.

The 1/6 scale steel strut model is shown in Fig. 2. The two rocket nozzles transition from a round cross section to a square exit (0.833 inches × 0.833 inches). The rocket nozzles have an area ratio of 4.529 (accounting for corner fillets). The thin, two-dimensional turbine exit (0.488 inches × 0.09 inches) is embedded in the strut between the rocket nozzles. The exit plane of the turbine is approximately 0.23 inches upstream of the rocket nozzle exit plane. This configuration was designed to enhance vertical mixing between the turbine and the rocket exhaust flows. The turbine nozzle has an area ratio of 1.126. Based on the requirement to match convective Mach number, the rocket nozzles were designed to exit at approximately standard atmospheric pressure (14.7 psia). The turbine was designed to exit at approximately twice this value. The strut is 7 inches long. An aerodynamic fairing approximately 2.25 inches long is mounted upstream of the strut to streamline the flow around it.

The strut is mounted in a rectangular duct (approximately 4 inches tall × 3.5 inches wide) (Figs. 2 and 3) with an aluminum top and bottom and transparent plexiglass sidewalls. The sidewalls are modular with interchangeable sections to allow easy access to the inside of the duct and direct observation of the flow. The installed strut reduces the duct open area by approximately 30%. As shown in the photo of Fig. 4 and schematically in Fig. 5, the duct has an elliptically contoured, two-dimensional bellmouth inlet open to the atmosphere providing a smooth ingested airflow. It is oriented with the longest dimension parallel to the strut. The rear end of the duct exhausts into a 10-inch diameter sheet metal pipe diffuser. The upstream end of the diffuser is open to allow extra air to be drawn into and decelerate the exhaust jet. The diffuser discharges the flow into free air.

Table 1 Pressure instrumentation

Probe Type/Location	Pressure range, psia	Accuracy, psia
Static at inlet/duct junction	0 - 30	± 0.09 (0.3% F.S.)
Pitot at inlet/duct junction	Not Used	--------
Static in strut fairing	0 - 30	± 0.09 (0.3% F.S.)
Pitot in strut fairing	0 - 30	± 0.09 (0.3% F.S.)
Static in duct/strut gap sidewall	0 - 15	± 0.03 (0.2% F.S.)
Pitot surveys	0 - 300	± 0.6 (0.2 % F.S.)

Instrumentation

The systems supplying air to the model are instrumented to monitor the operating conditions (temperatures and pressures) during the experiment. The primary air supply measurement locations are shown in Fig. 1. As shown in Fig. 5, the flow path is instrumented to measure static and total pressure where the inlet and duct meet and the sidewall static pressure in the duct/strut gap. A pitot-static tube is mounted through the strut fairing at the centerline of the duct. The tube protrudes into the flow about 1-inch upstream of the fairing. The measured pitot and static pressures were used to calculate the dynamic pressure of the ingested flow. The pressure ranges of the flow path transducers are summarized in Table 1. The pressure and temperature in the simulated 'combustion' chambers of all three nozzles are measured and recorded during each test. The pressure measurement in the rocket chamber is also used for feedback control of the regulating valve in the air supply system.

Results and Discussion

In the air-augmented rocket mode the embedded rocket exhausts (primary flow) create a pumping (ejector) effect that induces a secondary flow through the inlet. Characterizing the ejector effectiveness is critical to understanding the primary and secondary flow mixing and predicting overall system performance. A series of tests were run in the UAH Strutjet facility with rocket chamber pressures up to 600 psia and primary mass flow rates (both rockets) up to 4 lbm/sec.[5] The turbine flow was seeded with acetone vapor and a planar laser induced fluorescence

(PLIF) technique was used to obtain images of the rocket/turbine jet mixing. These images are presented in a companion paper.[6] There are various features in the PLIF images that are not fully understood. Therefore, a complementary study of the induced flow has been initiated. The current status of this study is presented in the following sections.

Induced Mass Flow

A primary question is whether the secondary (induced) flow is choked. Choking can occur through one of two mechanisms, a traditional area choke or a Fabri mass choke.[7] A traditional choke occurs when the flow is restricted through a minimum area. For the Strutjet, this minimum area is located in the gap between the strut and the sidewall. The duct area is reduced approximately 30% due to the strut and the effective area is evening smaller when the boundary layer is considered. A Fabri choke occurs when the blockage of the primary jet creates an effective minimum area in the duct (mixing tube) that chokes the secondary flow.

The presence of a choked secondary flow can be determined by direct mass flow measurements. However, this is impractical in the Strutjet facility. Therefore, the mass flow rate was calculated from the measured dynamic pressure ahead of the strut fairing. The Pitot (Po) and static (p) pressures ahead of the fairing were measured independently. Using isentropic relations it was determined that the Mach number ahead of the strut never exceeds 0.4. Therefore, the incompressible Bernoulli equation can be rearranged to calculate the local core flow velocity by

$$V = \sqrt{\frac{2(P_o - p)}{\rho}}, \qquad (1)$$

where V is the velocity of the ingested air, ρ is the density calculated from the ambient conditions, Po is the measured total pressure, and p is the measured static pressure. The approximate mass flow rate is then determined from the calculated velocity and density and the known cross sectional area.

Based on isentropic flow theory for choked nozzles, the rocket mass flow rate in lbm/sec can be estimated by

$$\dot{m}_{rocket} = \frac{0.532 A^* P_o}{\sqrt{T_o}}. \qquad (2)$$

The constant 0.532 accounts for the effects of gamma and the specific gas constant of air, and unit conversions. A^* is the rocket nozzle throat area in *square inches*, Po is the nozzle chamber pressure in *psia*, and To is the chamber temperature in °R.

Figure 6 shows the evolution of the induced flow dynamic pressure ($q = Po - p$) as the rocket chamber pressure is increased to a set point of 600 psia. For this initial test the air was not heated and was at an estimated temperature of 480 °R. At a rocket chamber pressure of approximately 250 psia the induced flow dynamic pressure becomes constant. This indicates that the secondary flow has choked. Figure 7 compares the calculated mass flow rates for the secondary and primary (both rockets) flows based on Eqs. (1) and (2), respectively. As expected, the induced mass flow increases with increasing rocket mass flow rate. The secondary flow chokes at approximately 2.4 lbm/sec when the total rocket mass flow rate is approximately 2 lbm/sec. This corresponds to a rocket chamber pressure of approximately 275 psia. The upper curve in Fig. 7 indicates the mass flow as the rocket pressure is ramped up. The lower curve shows the decrease in secondary mass flow as the rocket pressure decreases. Not surprisingly, initiating the secondary flow follows a different process than "unstarting" the flow.

Flow Visualization

Several flow visualization tests were performed to investigate the presence of flow structures such as shock waves, shear layers, and plume impingement on duct sidewalls. In one series shadowgraph images of the strut exit plane region were obtained. Only the rockets were run at pressures of 250, 275, 300, and 550 psia. Both room temperature (≈ 530°R) and heated air (≈ 760°R) were used. Fig. 8 shows the shadowgraph for a chamber pressure and temperature of 550 psia and 530°R, respectively. The locations of the rocket nozzles and the strut exit plane are indicated. The vertical lines are scores on the sidewall plexiglass that are approximately 1/2, 1, and 2 inches from the strut exit plane. A barrel shock is seen in both nozzle plumes. These shocks are believed to emanate from the contour curvature discontinuity where the nozzle cross-section transitions from round to square. The shocks initially spread indicating the nozzles are underexpanded. Asymmetry due to nozzle plume interactions is also evident. The shadowgraph resolution is not adequate to capture shear layer features. The low temperatures in the expanded plumes caused water condensation on the duct walls. The black spot on the left side of the shadowgraph is a result of this.

In the next test series carbon black (a kerosene-graphite mixture) was coated on the bottom of the duct. As the rocket pressure increases, the kerosene is evaporated into the induced duct flow leaving traces of graphite. The graphite "trails" provide simple imaging of flow structures in the duct. The tests used rockets only and room temperature air (the flash point of carbon blacking is 600°R). Still photographs and video images were taken. Since the pressure measurements indicate that the secondary flow chokes between 200 and 300 psia, the higher pressure was tested first. During ramp up to 300 psia, video images indicated a shock originating near the strut and traveling downstream, scrubbing off a large portion of the graphite. This is believed to be a starting shock that initiates a supersonic secondary flow. Figure 9 shows the duct sidewall after the 300-psia test. In the next test the rockets were ramped up to 250 psia. Video images indicated no shock wave generation in the duct at this pressure. Figure 10 shows the duct sidewall after this test. Comparing Figures 9 and 10, the shock wave at a rocket pressure of 300 psia scrubbed off much of the graphite in the duct. Based on these tests, it is believed that the flow experiences a traditional choke due to the minimum area in the duct/strut gap region.

Pressure Surveys

In the next test series a set of pressure traverses were performed. One purpose of these tests was to investigate the flow in the duct/strut gap region where choking is believed to occur. The other objective was to investigate the rate rocket and turbine plume expansion. This information can be used to interpret the PLIF images of the rocket/turbine jet mixing as well as evaluate of expansion losses in the mixing region. Three Pitot tubes were mounted to a Unislide automatic traversing mechanism and translated normal to the duct flow. The tubes have an outer diameter of approximately 0.125 inches. Hypodermic needles were mounted in the tubes to increase spatial resolution and reduce noise in the pressure readings. The tubes were positioned vertically as follows (see Fig. 2): probe 1 is on the horizontal center-line of the top rocket nozzle; probe 2 is on the horizontal center-line of the turbine nozzle; and probe 3 is on a line that traverses the strut below the bottom rocket nozzle exit. As noted in Table 1, each tube was connected to a 300-psia transducer.

As denoted in Fig. 5, traverses were conducted at two stations within the duct/strut gap: (1) 3.875 inches upstream of the strut exit (near the sidewall static port); and (2) 3 inches upstream of the strut exit. Traverses were also made at the strut exit, 1-inch downstream of the strut and 4.25 inches downstream of the strut. Two or three traverses were made at each station. In each test the rocket chamber pressure was ramped up to a set point and held constant while a traverse was performed. The pressure was then ramped up to the next set point and the traverse was repeated. Traverses were performed at rocket pressures of 200, 275, 366, and 550 psia. There was a noticeable blockage effect as the tubes traversed into the duct. Therefore, the tubes were traversed from the duct sidewall in to the strut wall or duct centerline and then back. Because of the large radius of the tube elbows, the tubes could only be brought to within approximately 0.2 inches of the duct sidewall. The tubes could be brought to within approximately 0.0625 inches of the strut wall. The pressure traverse data was reduced to a moving time averaged curve. Ten points were averaged to reduce the noise in the data.

Figure 11 shows histories for the various operating and duct pressures measured during a traverse in the gap region 3 inches upstream of the strut exit plane. The set point and actual rocket chamber pressures are shown reduced by a factor of 100. It can be seen that the chamber pressure fluctuates as much as ± 15 psi around the set point. The total pressure measured ahead of the fairing remains constant at approximately 14.75 psia throughout the test. The static pressures at the inlet/duct transition and ahead of the fairing are essentially the same. They reflect the variation in rocket chamber pressure especially at 200 and 275 psia. The fairing static pressure is essentially constant at 366 and 550 psia, indicating the secondary flow has choked. This can also be seen in the dynamic pressure ahead of the fairing. The static pressure at the duct sidewall port in the strut gap also shows a significant effect due to the variations in rocket chamber pressure. As the Pitot probes are traversed into the strut gap, the wall static pressure rises. This indicates the significant blockage effects of the probes.

Figure 12 is a pressure history plot measured during a traverse 4.25 inches downstream of the strut exit plane. Most of the pressure traces are similar to those of Fig. 11. However, the sidewall static pressure is approximately 20% lower for this case than for the traverse in the strut gap.

Figures 13 - 21 show the Pitot pressure surveys at various locations along the duct for rocket chamber pressures of 200 and 550 psia. The duct sidewall is at 0 and the centerline is at 1.75 inches. The strut edge is at 1.25 inches and the edge of a rocket nozzle is at 1.33 inches. The Pitot pressures are normalized by the total pressure measured ahead of the strut fairing. This reference was chosen in order to determine where the secondary flow becomes supersonic. In a supersonic

flow a normal shock will form ahead of the Pitot probe. This will result in a drop in total pressure that can be correlated to a local Mach number. In a subsonic flow the total pressure drop is due to viscous dissipation in regions of high shear (i.e., boundary layers and mixing layers).

The traverses in the duct/strut gap are shown in Figs. 13 - 16. Because of the large radius of the tube elbows, the boundary layer on the duct sidewall was not captured. As expected, the strut boundary layer is small in the vicinity of the rocket and turbine nozzles. Probe 3 indicates a relatively thick boundary layer in the corner flow near the base of the strut. There is an identifiable core flow within the gap. Unfortunately, the resolution of the 300-psia traverse probe transducers is not sufficient to accurately determine the local Mach number. However, it is believed that when the secondary flow is choked, the sonic line lies closer than 3 inches to the strut exit plane.

Figures 17 - 21 are pressure survey plots at the strut exit plane, 1 inch downstream, and 4.25 inches downstream. Pressures in the strut exit plane at 200 psia are shown in Fig. 17. Two separate traverses are plotted and indicate good repeatability. All three probes show a uniform core flow until near the strut edge at 1.25 inches. The trace across the upper rocket nozzle (Probe 1) then shows an initial increase in pressure as the probe moves through the shear layer between the gap flow and higher pressure rocket plume. The pressure then drops to a relatively constant level through most of the nozzle core. The design condition for the rocket nozzle area ratio of 4.529 yields an exit Mach number of approximately 3.08. However, the measured total pressure is 1/2 what it should be based on normal shock relations. At this chamber pressure the rocket nozzles may be overexpanded and have internal normal shocks. The trace across the turbine centerline exhibits a complex pattern of three peaks that extends much wider laterally than the turbine nozzle edge at 1.705 inches. The total pressure measured at the center of the turbine exit is also significantly less than predicted by normal shock relations. This pattern may be due to the complex mixing between the embedded turbine plume and the rocket flow. The sharp corners where the turbine slit meets the rocket exit plane may also generate vortices. Another concern is that the relatively large probe may represent significant blockage in the turbine exhaust plane. Probe 3 shows a slight total pressure drop as it moves across the wake at the strut base.

Figure 18 shows the pressure traces in the strut exit plane for a rocket chamber pressure of 550 psia. Probe 1 indicates that the rocket plume has not spread laterally beyond the strut width. The total pressure decreases slightly then rises through the plume boundary. The pressure next dips sharply as it passes through the barrel shock that was seen in the shadowgraph of Fig. 8. The total pressure then rises again until it peaks at the nozzle center. Using the measured centerline total pressure and normal shock relations, the nozzle exit Mach number is predicted to be 3.2. This value is consistent with the theoretical design value of 3.08 and lends confidence to the accuracy of the pressure measurements. Probe 2 again exhibits a complex flow pattern in the turbine exhaust region. Probe 3 indicates a similar drop in pressure in the strut base wake as for the 200-psia case. However the strut wake appears to be slightly wider.

Figure 19 shows the pressure traces at 1 inch downstream of the strut exit plane for a rocket chamber pressure of 550 psia. Probe 1 shows that the rocket plume has expanded laterally into the secondary flow and the core pressure has decreased significantly. The peak that is believed to be due to the barrel shock has moved laterally. Probe 2 indicates that the turbine exhaust has also spread laterally. But the peak total pressure level is still very high. In fact it exceeds the total pressure of the air delivered to the turbine. Probe 3 indicates that the base wake has spread further. In addition, a significant pressure spike has appeared at a location 1 inch from the duct sidewall. The traces exhibited by Probes 2 and 3 may be due to a complex interaction between the exhaust plumes, wakes, and possible shock structures in the mixing region. However, these patterns also bring into question the accuracy these pressure measurements.

Figures 20 and 21 show the pressure traces 4.25 inches downstream of the strut exit plane at rocket chamber pressures of 200 and 550 psia, respectively. At this station the plumes for the 200 psia case (Fig. 20) have significantly expanded and mixed with the secondary flow. At 550 psia (Fig. 21) the rocket plume pressure trace is still significant. There still appears to be a possible shock structure at approximately 1.5 inches from the duct sidewall. Probes 2 and 3 exhibit similar features to the traces at 1 inch, however the peak pressure levels are lower. One other important feature can be noted at this location. The total pressure ratio measured in the core of the secondary flow outside the rocket plume (Probe 1) indicates a supersonic Mach number even when the measurement uncertainty is considered.

Comparison to Previous Research

A literature search indicated that there are significant differences between the current investigation and previous ejector studies. These studies primarily investigated axisymmetric configurations for

the mixing tubes and the nozzles. The UAH Strutjet configuration consists of a rectangular duct and square rocket nozzle exits. Also the strut represents a much larger blockage to the induced flow-field. The UAH rocket nozzle chamber conditions and flow rates are also much higher than the conditions previously investigated. In the classic work by Fabri and Sistrunk[7] the ratio of rocket chamber total pressure to secondary stream total pressure was limited to a maximum $Po_{rocket} / Po_{ingested} = 6$. Supersonic flow due to a Fabri mass choke for this pressure ratio occurs when $\dot{m}_{ingested} / \dot{m}_{rocket} \approx 0.22$. The current system has a maximum ratio pressure ratio of approximately 40, and $\dot{m}_{ingested} / \dot{m}_{rocket} \approx 0.6$. Also, NASA funded studies in the 1970's on single nozzle ejector systems with a circular mixing tube had maximum nozzle mass flow rates of 0.12 lbm/sec[8]. A total nozzle mass flow rate of 4 lbm/sec is used in the UAH Strutjet study.

Conclusions and Future Work

This paper summarizes the current status of a research effort to characterize the rocket induced flow in a Strutjet simulation facility. Various flow visualization tests and pressure surveys have been performed. Pressure measurements indicate that the secondary flow induced in the rectangular duct by the primary rockets chokes when the rocket chamber pressure is between 200 and 300 psia. Flow visualization studies indicate the propagation of a starting shock in the duct as the rocket pressure is ramped up to 300 psia. The secondary flow choking is believed to be due to the minimum area in the duct/strut gap and not due to a mass addition. Several total pressure surveys have also been made in the strut gap and the plume mixing region. These surveys indicate a complex flow structure including barrel shocks and possibly vortices. pressure traverses indicated the complexity of the flow in the supersonic rocket exhaust.

Future work will consist of repeating the pressure surveys with higher resolution instrumentation. This includes smaller diameter probes and higher precision pressure transducers. A CFD model of the induced flow is also being developed. Finally, tests of a single nozzle strut and other nozzle configurations are planned.

Acknowledgements

The UAH Strutjet research facility was constructed with funding from NASA Grant NCC8-123. Ms. Thames was funded under the NASA Graduate Student Researchers Program, Grant NGT8-52855. The authors would like to acknowledge the assistance of UAH graduate students Matt Turner and Jim Lambert.

References

1. Bulman, M., and Siebenharr, A., "The Strutjet Engine: Exploding the Myths Surrounding High Speed Airbreathing Propulsion", *AIAA 95-2475*, July 1995.
2. Siebenhaar, A., and Bulman, M.J., "The Strutjet Engine: *The Overlooked Option for Space Launch*", *AIAA 95-3124*, July 1995.
3. Parkinson, D, Turner, M and Wagner, D, "Mixing of Hypersonic Streams", *AIAA 99-2454*, June 1999.
4. Spetman, D. M., Hawk, C. W. and Moser, M. D., "*Development of a Strutjet Cold-Flow Mixing Experiment*", ***Journal of Propulsion and Power***, Vol. 15, No. 1, January-February 1999, pp. 155-158.
5. Hawk, C.W., Landrum, D.B., Spetman, D., and Parkinson, D., "Mixing of Supersonic Streams", *Proceedings of the 1998 JANNAF Joint Meeting of the Combustion, Propulsion System Hazards, and Airbreathing Propulsion Subcommittees*, Cleveland, OH, July 1998.
6. S. Muller, C. W. Hawk, P. G. Bakker, D. Parkinson and M. Turner, *"Mixing of Supersonic Jets in a RBCC Strutjet Propulsion System"*, AIAA Paper 99-2973, AIAA/SAE/ASME/ASEE 35th Joint Propulsion Conference and Exhibit, Los Angeles, CA, June 1999
7. Fabri, J., and Siestrunck, R., "Supersonic Air Ejectors", Advances in Applied Mechanics, Vol. V, Academic Press, New York, 1958, pp. 1-34.
8. Hickman, Kenneth E., Hill, Philip G., and Gilbert, Gerald B., "Analysis and Testing of High Entrainment Single-Nozzle Jet Pumps with Variable-Area Mixing Tubes", NASA-CR-2067, June 1972.

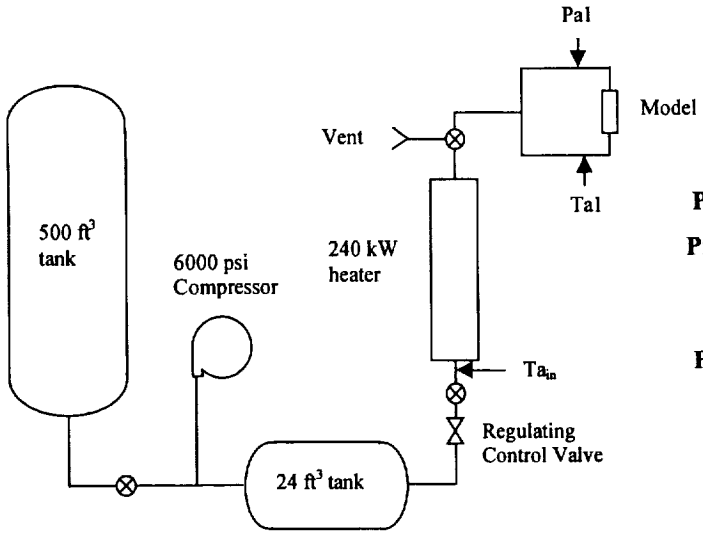

Fig. 1 Air supply system for UAH Strutjet simulation facility.

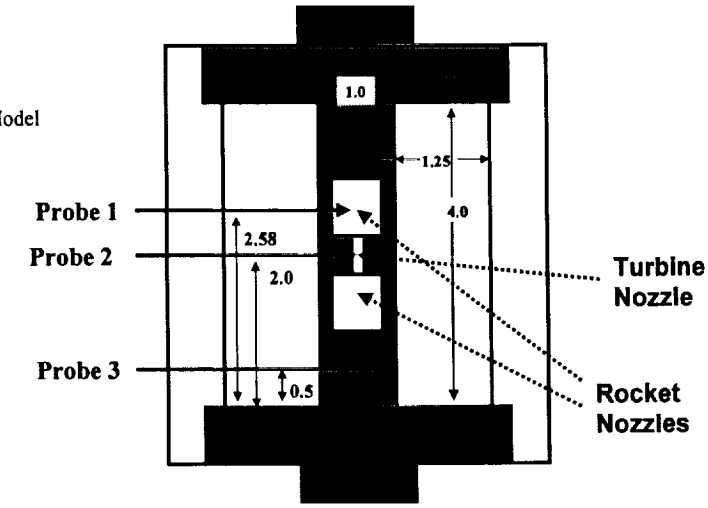

Fig. 2 Strut model geometry and pressure survey locations.

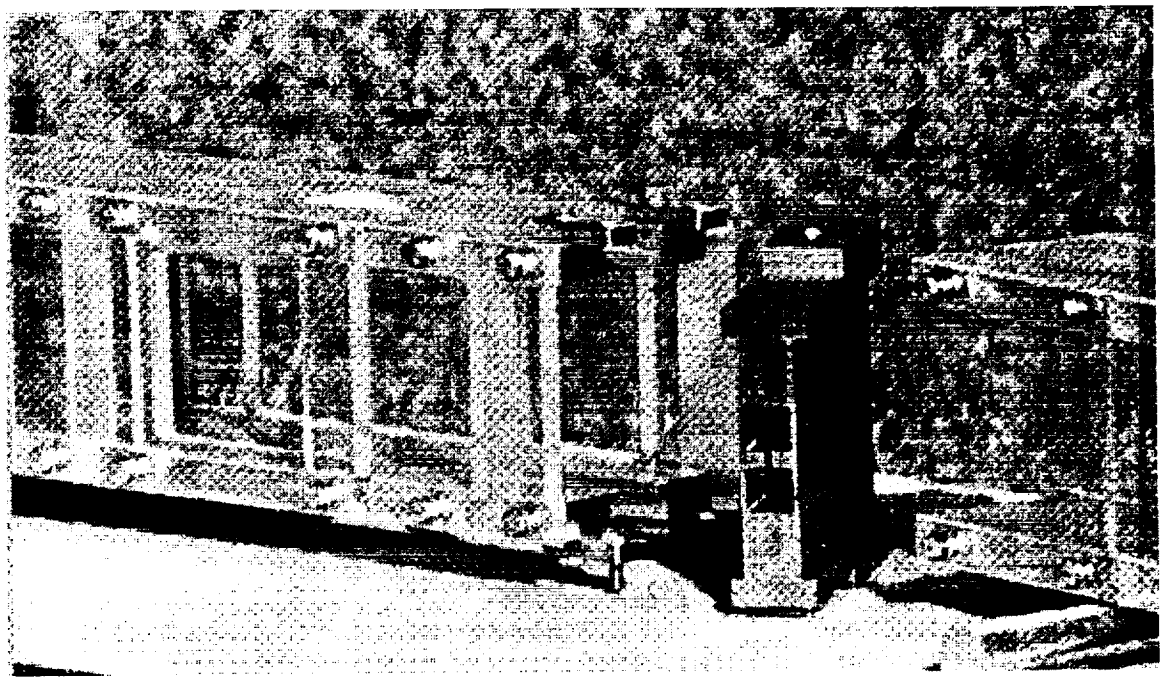

Fig. 3 Disassembled duct and strut model . Note square rocket nozzle exits and embedded turbine nozzle exit slit.

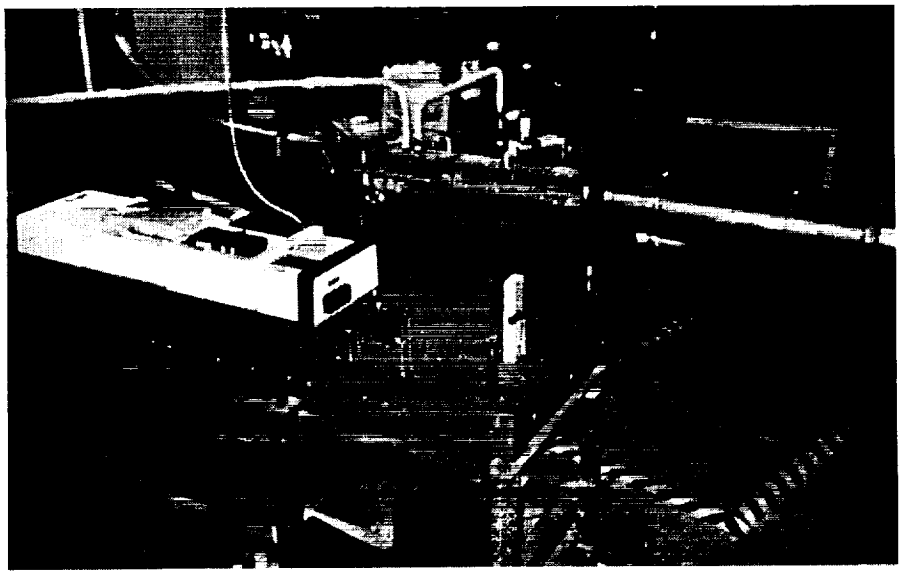

Fig. 4 UAH Strutjet simulation facility showing contoured inlet, duct, diffuser, and diagnostics table.

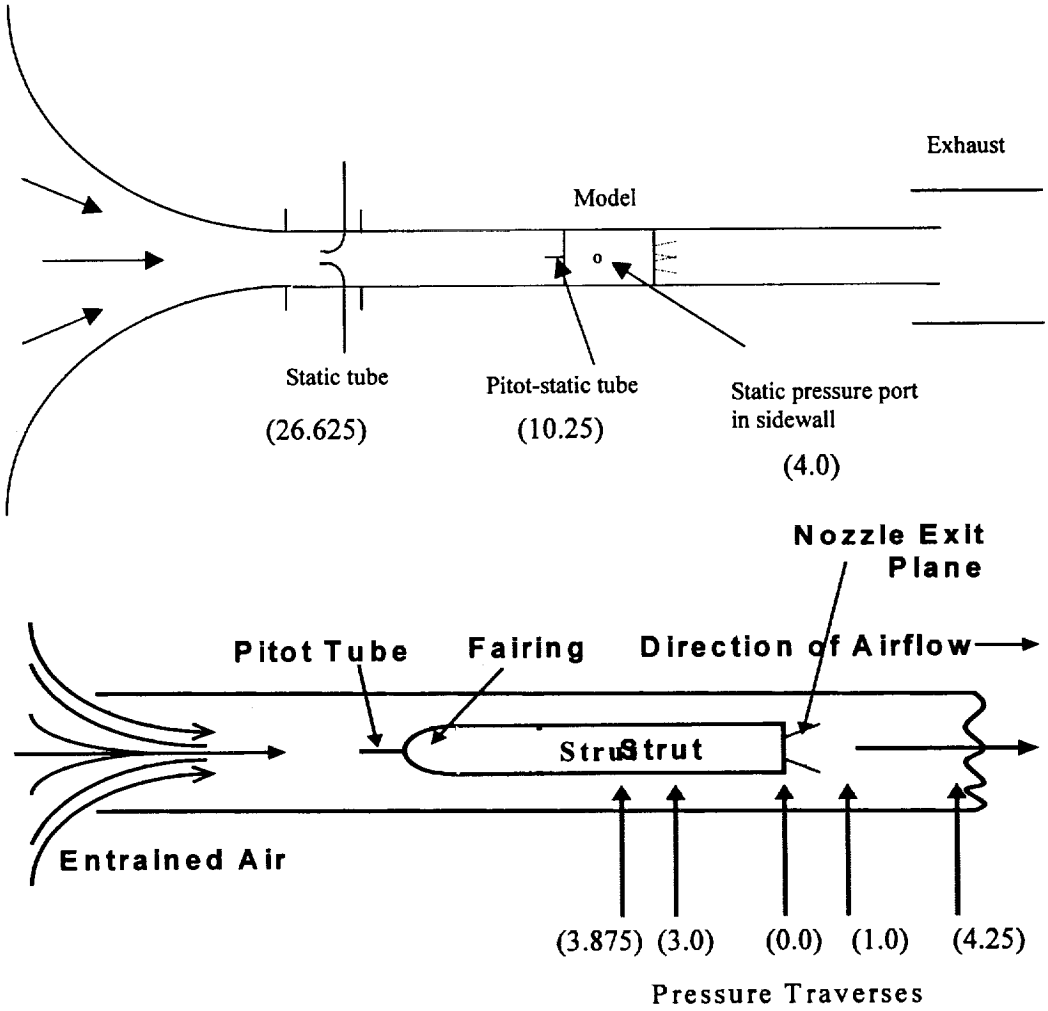

Fig. 5 Schematics (not to scale) of Strutjet facility including pressure measurement and survey locations. Dimensions are in inches and relative to strut exit plane.

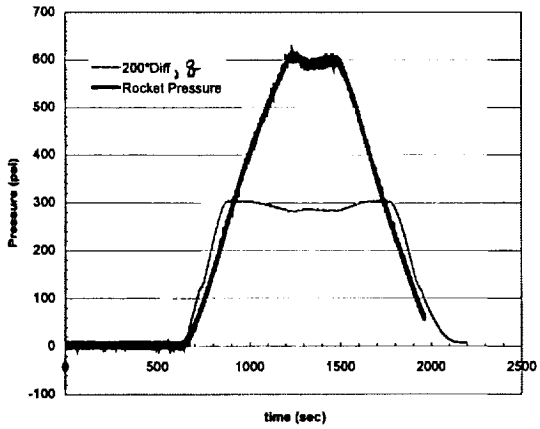

Fig. 6 Rocket chamber pressure and secondary (induced) flow dynamic pressure histories.

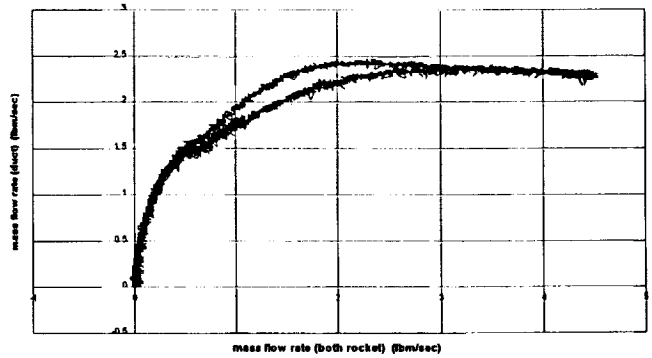

Fig. 7. Calculated secondary mass flow rate versus total rocket mass flow rate.

Fig. 8 Shadowgraph of strut exit region with rockets alone operating at *Po* = 550 psia and *To* = 580°R.

Shadowgraph Description

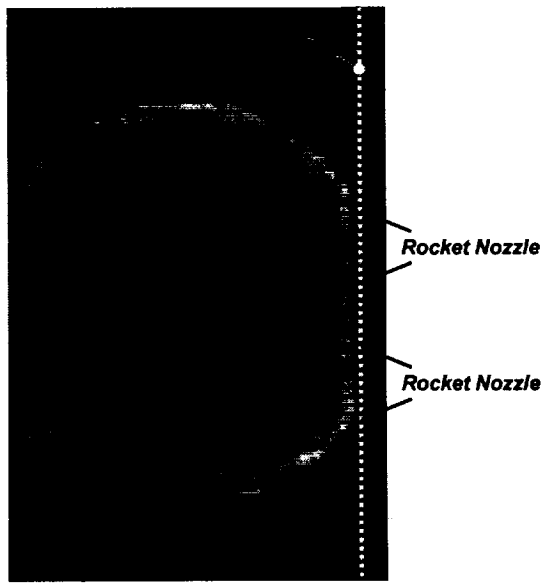

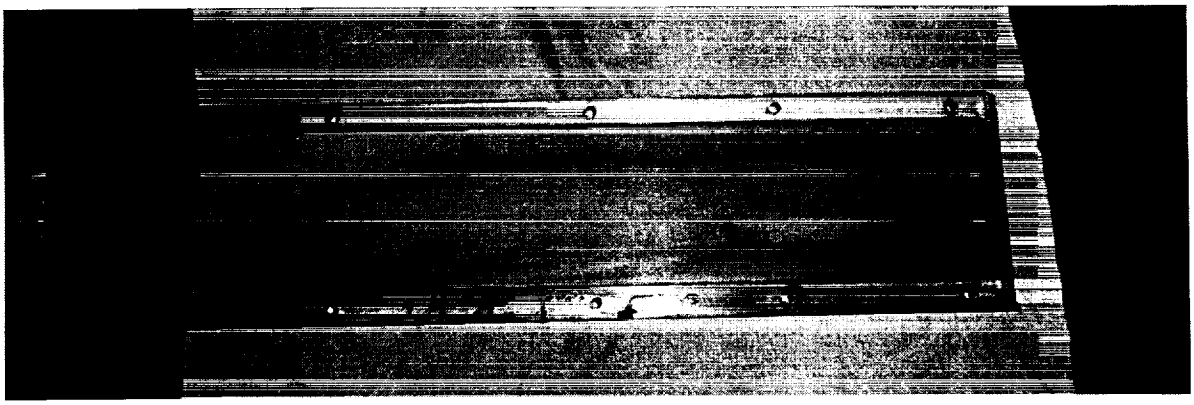

Fig. 9 Carbon black on duct sidewall after 300 psia rocket pressure run.

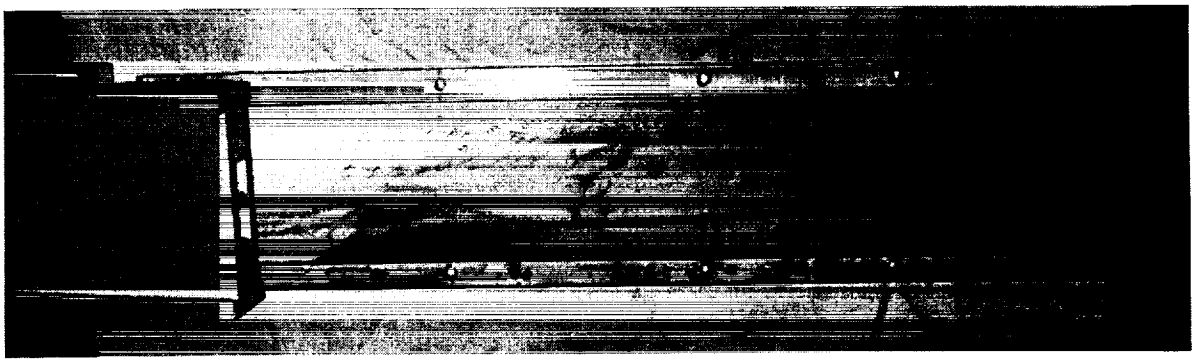

Fig. 10 Carbon black on duct sidewall after 250 psia rocket pressure run.

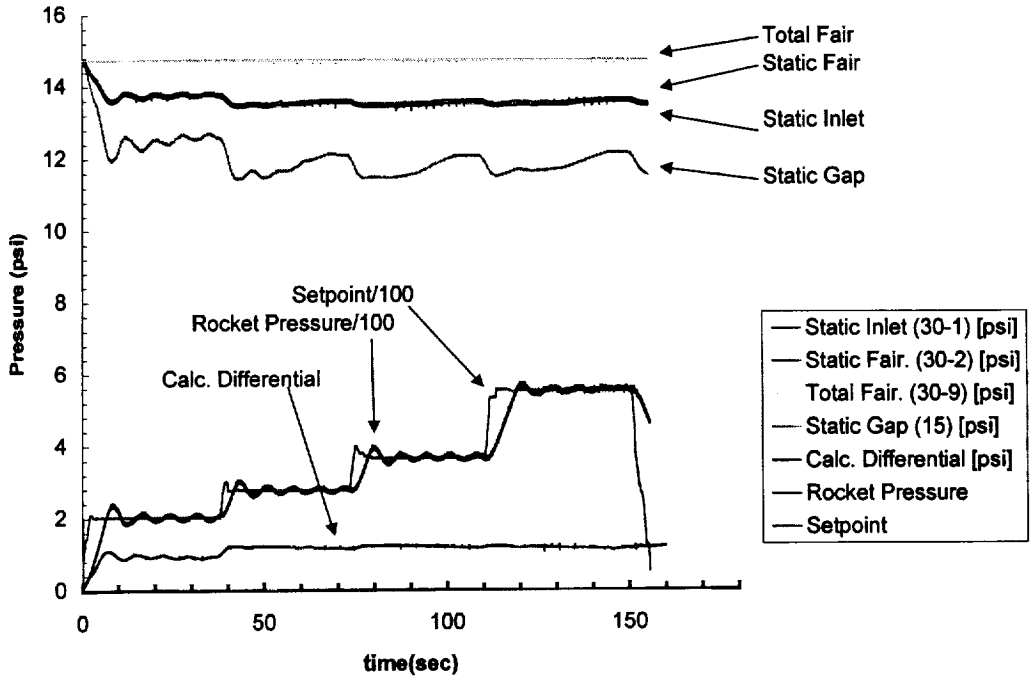

Fig. 11 Operating and duct pressure histories during pressure traverse in the strut gap 3 inches upstream of the strut exit plane.

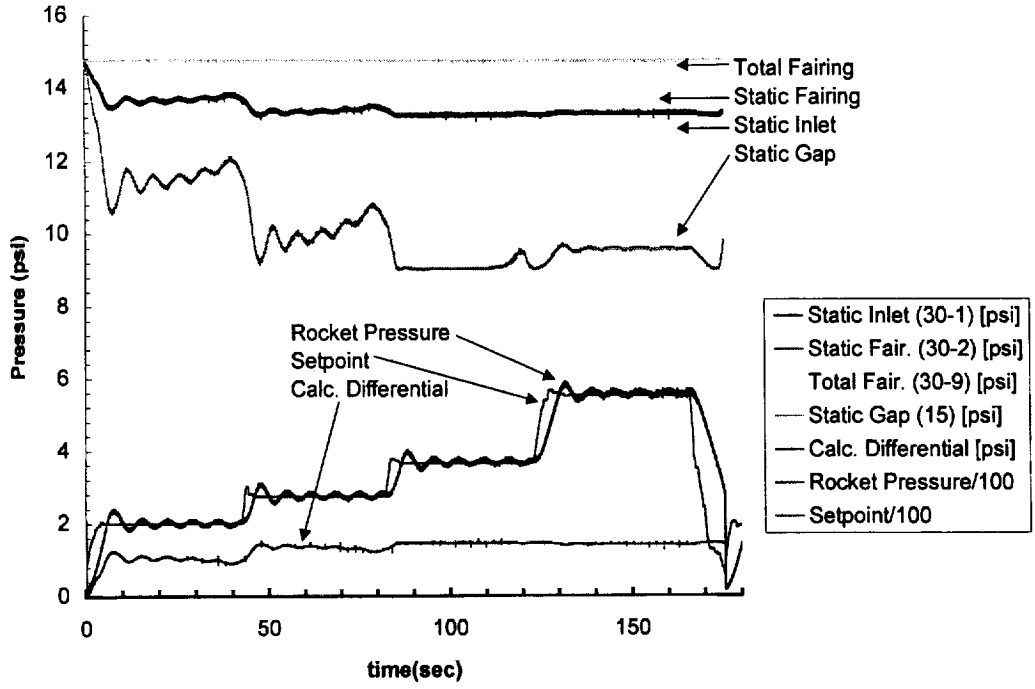

Fig. 12 Operating and duct pressure histories during pressure traverse 4.25 inches downstream of the strut exit plane.

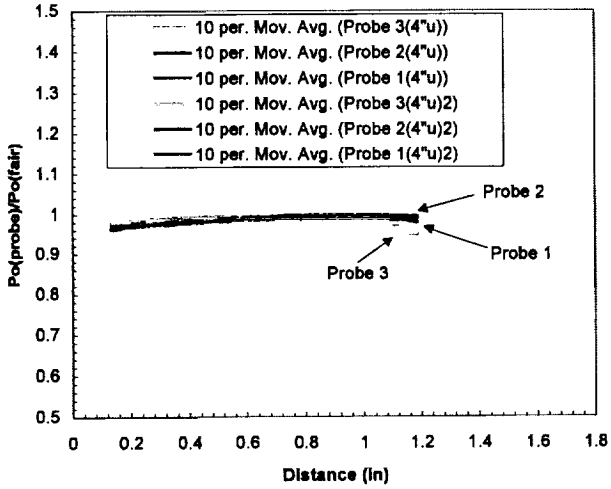

Fig. 13 Pressure survey in strut gap 3.875 inches upstream of strut exit plane. Rocket chamber pressure is 200 psia.

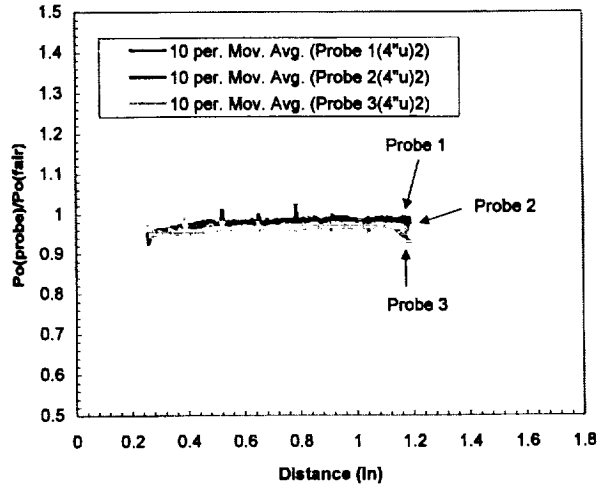

Fig. 14 Pressure survey in strut gap 3.875 inches upstream of strut exit plane. Rocket chamber pressure is 550 psia.

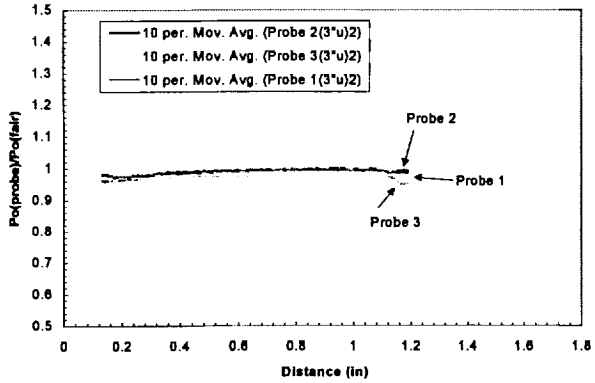

Fig. 15 Pressure survey in strut gap 3 inches upstream of strut exit plane. Rocket chamber pressure is 200 psia.

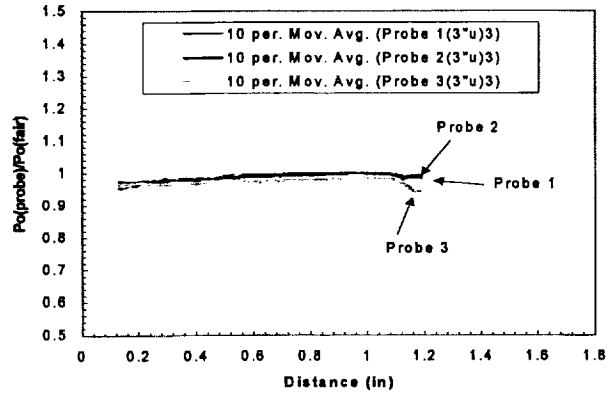

Fig. 16 Pressure survey in strut gap 3 inches upstream of strut exit plane. Rocket chamber pressure is 550 psia.

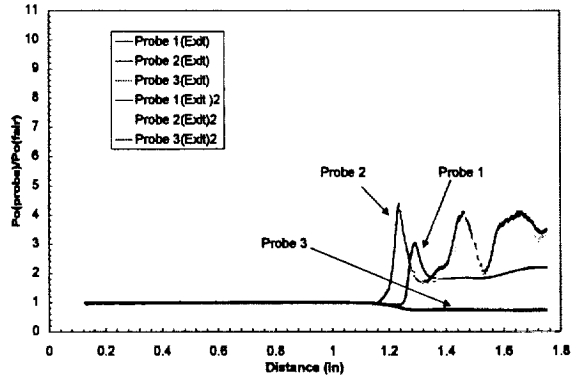

Fig. 17 Pressure survey at strut exit plane. Rocket chamber pressure is 200 psia.

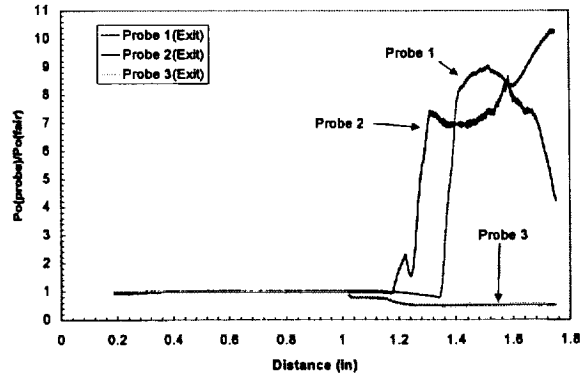

Fig. 18 Pressure survey at strut exit plane. Rocket chamber pressure is 550 psia.

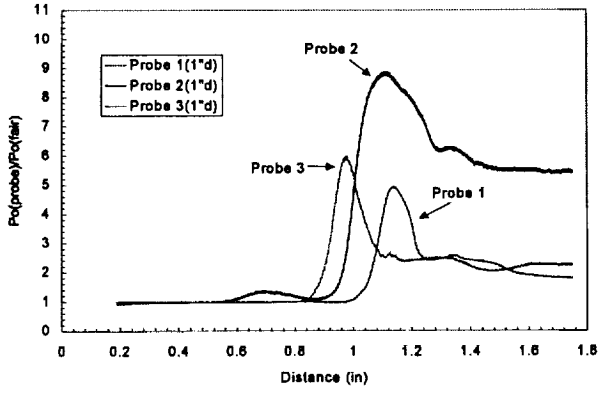

Fig. 19 Pressure survey 1 inch downstream of strut exit plane. Rocket chamber pressure is 550 psia.

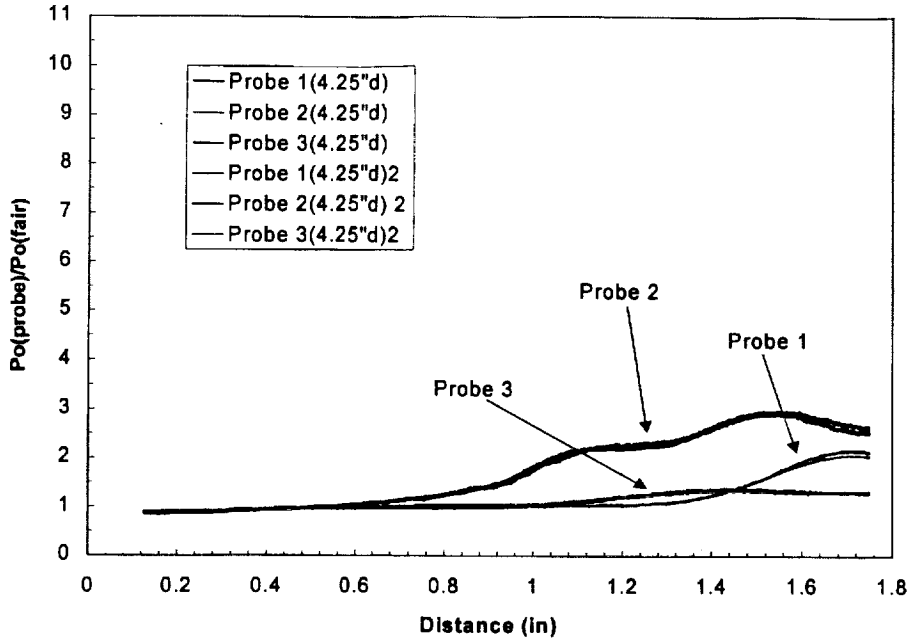

Fig. 20 Pressure survey 4.25 inches downstream of strut exit plane. Rocket chamber pressure is 200 psia.

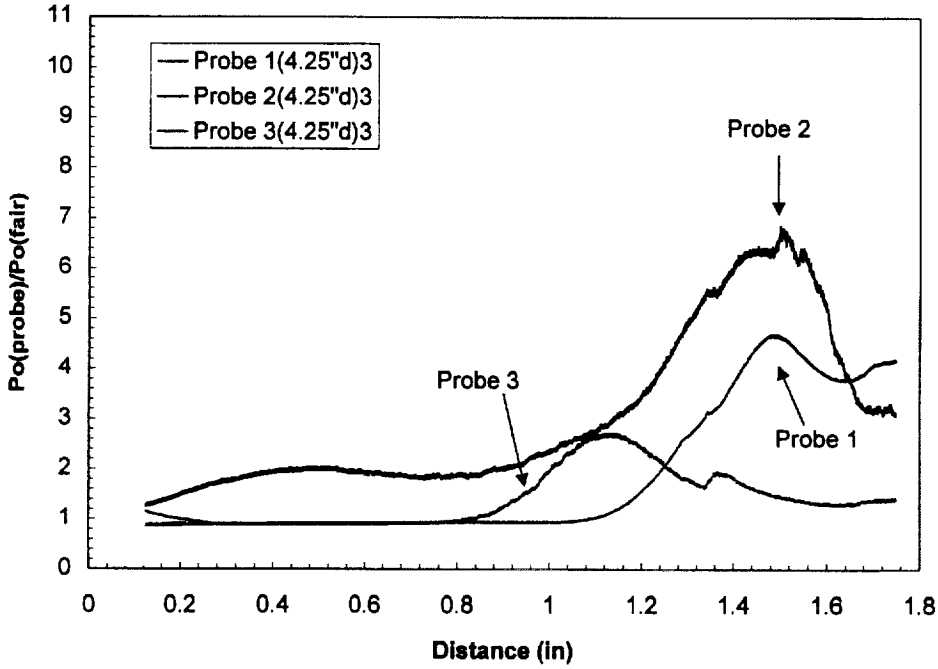

Fig. 21 Pressure survey 4.25 inches downstream of strut exit plane. Rocket chamber pressure is 550 psia.